Directing Energy Transfer in Pt(bodipy)(mercaptopyrene) Dyads

Peter Irmler,[†] Franciska S. Gogesch,[†] André Mang,[†] Michael Bodensteiner,[‡] Christopher B. Larsen,[§] Oliver S. Wenger,[§] and Rainer F. Winter[,†]*

[†]Fachbereich Chemie, Universität Konstanz, Universitätsstraße 10, D-78457 Konstanz, Germany

[‡]Fakultät für Chemie und Pharmazie, Universität Regensburg, Universitätsstraße 31, D-93053 Regensburg, Germany

[§]Department of Chemistry, University of Basel, St.-Johanns-Ring 19, CH-4056 Basel, Switzerland.

NIR Phosphorescence, Panchromatic Absorber, Platinum, Singlet Oxygen, Bodipy, Pyrene, Dyad.

Abstract: We report on the photophysical properties of three dyads that combine a 4,4-difluoro-4-bora-3a,4a-diaza-*s*-indacene (bodipy, BDP) and a mercaptopyrene (SPyr) dye ligand at a $Pt(PEt_3)_2$ fragment. σ-Bonding of the dyes to the Pt ion promotes intersystem crossing (ISC) via the external heavy atom effect. The coupling of efficient ISC with charge-transfer from the electron-rich mercaptopyrene to the electron-accepting BDP ligand (PB-CT) gives rise to a multitude of (potentially) emissive states. This culminates in the presence of four different emissions for the mono- and dinuclear complexes **BPtSPyr** and **BPtSPyrSPtB** with an unsubstituted BDP ligand and either a terminal 1-mercaptopyrene or a bridging pyrene-1,6-dithiolate ligand. Thus, in fluid solution, near IR emission at 724 nm from the ^{3}PB-CT state is

observed with a quantum yield of up to 15%. Excitation into the BDP-based $^1\pi\pi^*$ or the pyrene-based $^1\pi\pi^*$ band additionally trigger fluorescence and phosphorescence emissions from the BDP-centred $^1\pi\pi^*$ and $^3\pi\pi^*$ states. In frozen solution, at 77 K, phosphorescence from the pyrene ligand becomes the prominent emission channel, while PB-CT emission is absent. Alkylation of the BDP ligand in **KBPtSPyr** funnels all excitation energy into fluorescence and phosphorescence emissions from the KBDP ligand. The assignments of the various excited states and the deactivation cascades were probed by absorption and emission spectroscopy, transient absorption spectroscopy, electrochemical and UV/Vis/NIR spectroelectrochemical measurements, and by quantum chemical calculations. Our conclusions are further corroborated with the aid of suitable reference compounds comprising of just one chromophore. All dyads are triplet sensitizers and are able to generate singlet oxygen.

Introduction

Luminescent molecules capable of displaying multiple emissions are of great interest, e. g. as one-component white-light emitters,[1-4] and, in the case of dual fluorescence and phosphorescence emitters, as one-component sensors for triplet molecules. The latter quench selectively the longer-lived phosphorescence emission, while leaving the fluorescence unperturbed.[5-9] An observation of multiple emissions from the same compound obviously necessitates the presence and competitive population of two or more emissive states. One possible strategy to achieve dual fluorescence and phosphorescence emissions is to match the intersystem crossing (ISC) rate constant k_{ISC} to the fluorescence time constant k_f. According to El-Sayed's rule,[10, 11] this can be achieved by capitalizing on the large spin orbit coupling constant of a proximal heavy atom[12-15] or by admixing sufficient charge-transfer character to the underlying absorption. Both effects are capable of

changing the angular momentum of the excited electron.[11, 16-18] Alternatively, multiple emissions are also known for dyads with different electronically decoupled or weakly coupled chromophores.[19, 20] Examples of such a multichromophore approach with an ensuing competition between dye-based fluorescence and MLCT- or spin-orbit coupling- (SOC-) triggered phosphorescence emissions come from iridium, ruthenium, rhenium or platinum complexes that contain dye-modified cyclometalating,[21, 22] 2,2'-bipyridine or phenanthroline,[23-25] or alkynyl ligands.[18, 26-28] Phosphorescence quantum yields of such dyads are, however, usually lower than 10%.[24] Particularly impressive are $Ir(ppy)_2(Q)$ complexes with a 2-hydroxyquinoline ligand Q and two mutually orthogonally aligned, cyclometalated phenylpyridine (ppy) ligands, which show quadruple emissions comprising of ligand-localized fluorescence from the $^1n\pi^*$ and phosphorescence from ^{3}MLCT (MLCT = metal-ligand charge-transfer) states of the different ligands as a consequence of inefficient Förster resonance energy transfer.[29]

Platination of a dye, i. e. metal attachment via a direct Pt-carbon σ-bond, has been shown to be a viable means of accelerating ISC via the remote heavy atom effect,[15, 30, 31] in particular when using compact thioxanthone[32] or 4,4-difluoro-4-bora-3a,4a-diaza-*s*-indacene (BDP) dyes[8, 9, 33] (note that the remote heavy-atom effect scales with r^{-6}, where r denotes the distance between the heavy atom and the centre of gravity of the dye).[12] In this manner, quantum yields of up to 41% for dye-based phosphorescence emission in fluid solution at r.t. could be achieved. Complexes *trans*-$X(PR_3)_2Pt(BDP)$ (R = Ph, Et) were also found to be efficient sensors for the detection of triplet molecules and efficient photosensitizers for the production of singlet oxygen.[8, 9, 33, 34] An example of a panchromatically absorbing dyad of such a complex with an ethynylnaphthalimide (NI) dye as the anionic ligand X was also reported. The latter shows complete energy transfer from the locally excited ^{1}NI or ^{1}NI→BDP charge-transfer states to the lower-lying excited states of the BDP

ligand.[34] One drawback of this system, however, was its only limited stability under laser irradiation due to the mutual *trans*-arrangement of two carbyl ligands, which both exert a strong σ-trans influence.[9] We therefore sought to improve on this general architecture by attaching the second dye via a more robust Pt-thiolate bond. In doing so, we have chosen mercaptopyrenes as the second dye.

Pyrenes usually absorb in a spectral region where BDP dyes are almost transparent. Most pyrenes are highly fluorescent and show rather inefficient intersystem crossing with negligible phosphorescence quantum yields.[13, 35] The latter is a result of their long triplet-state lifetimes, which increases the probability of excited state decay by radiationless deactivation channels.[13] Pyrenes were already introduced into the coordination sphere of platinum ions, either by direct platination, or as ethynylpyrene ligands. In both cases, phosphorescence from the pyrene ligand could be obtained due to the proximity of the pyrene dye to the platinum ion, however with only modest quantum yields, even in frozen, glassy matrices.[15, 18, 21, 31, 36]

We note in this vein that pyrene-BDP dyads with a direct connection between the two different dyes have been known for more than ten years.[37, 38] More recently it was observed that these compounds, due to a near orthogonal arrangement of the pyrene donor and the BDP acceptor, are capable of forming a charge-separated (CS) excited state, which promotes efficient ISC to the corresponding ^{3}CS state. Such dyads are characterized by a strong dependence of their absorption and emission properties and their associated emission quantum yields on solvent polarity. They are capable of photogenerating singlet oxygen, sometimes with high quantum yields Φ_Δ, particularly in polar solvents. These ^{3}CS states are usually non-emissive though.[39-41]

Very recently we communicated our results on the complex **BPtSPyr**, which combines a *meso*-platinated BDP acceptor and a mercaptopyrene donor ligand at a common *trans*-Pt(PEt_3)$_2$ entity.[42] The most remarkable features of **BPtSPyr** are its multiple emissions and the dependence of its emission profile on the excitation wavelength, the solvent polarity, and the temperature. This behaviour indicates the presence of several competing pathways for the decay of the individual excited states to the ground state. Most prominent is the long-lived emission from the ^{3}CS state in the near infrared (NIR), which becomes observable due to an SOC-accelerated ISC rate for radiative decay from the corresponding T_1 to the S_0 state. We have now further elaborated on this complex by selectively manipulating the relative energies of the ^{3}CS and the ^{3}BDP excited states. This was done through either alkylation of the BDP ligand or through interlinking two *trans*-Pt(PEt_3)$_2$(BDP) fragments with a bridging 1,6-pyrenedithiolate ligand. These alterations have the effect of (re)directing the deactivation cascade to either BDP-localized or CS excited states. Suitable reference compounds, which contain only one of these two chromophores, were also included to aid in the understanding of their complex emissive behaviour. The results of this study are described herein.

Results and discussion

Synthesis. The general synthesis route is depicted in Scheme 1 (for detailed syntheses and NMR characterization and a brief discussion of the NMR spectroscopic trends see the Supporting Information (SI) and Figures S1-S21 as well as table S1 therein). The *meso*-Pt-BDP complexes were synthesized according to our previously reported protocol by oxidative addition of corresponding 8-chloro-BDP dye to the Pt^0(ethene)(PEt_3)$_2$ precursor.[8] The latter is generated in situ by thermally induced reductive elimination of ethane from the corresponding bis(ethyl) complex.[43] In the case of the peralkylated 8-chloro-krypto-BDP ligand KBDP, an elevated

temperature and longer reaction time were required in order for the oxidative addition to proceed, most probably as the result of a larger steric hindrance. Subsequent abstraction of the chlorido ligand with AgOTf followed by addition of the triflato complex to a solution of deprotonated 1-mercaptopyrene, or respectively, pyrene-1,6-dithiole, provided the target dyads in good to moderate yields.

Scheme 1. Exemplary synthesis of **KBPtSPyr** and the structures of all relevant compounds.

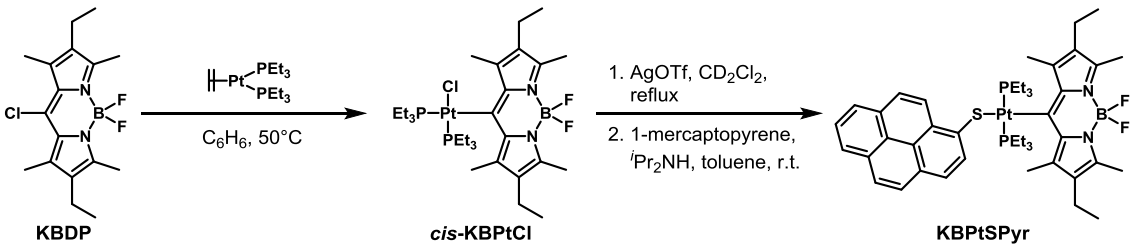

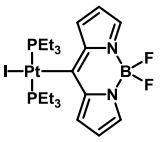
BPtI

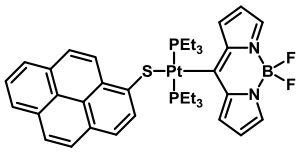
BPtSPyr

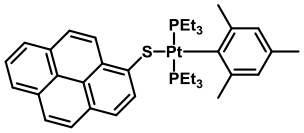
MesPtSPyr

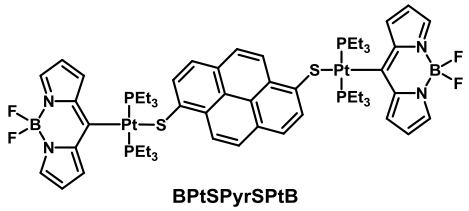
BPtSPyrSPtB

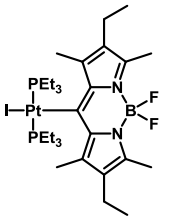
KBPtI

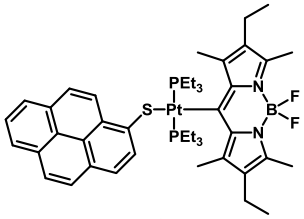
KBPtSPyr

The general pattern of resonance signals and, in particular, the observation of Pt-satellites for the appropriate proton and carbon resonances in the NMR spectra confirm the constitution of the

complexes and the presence of the Pt-C and the Pt-S bonds to the bodipy and mercaptopyrene ligands. Single crystals of **KBPtSPyr** and its precursor **KBPtI** for molecular structure determination by X-ray diffraction analysis were obtained by slow diffusion of *n*-pentane into saturated solutions of the complexes in CH_2Cl_2. Relevant crystal and refinement data are collected in Table S2 of the Supporting Information. Figure 1 depicts their molecular structures (only one of the two independent molecules in the unit cell of **KBPtSPyr** is shown), while Table S3 of the Supporting Information summarizes the most relevant bond parameters together with those of **BPtI**.[9]

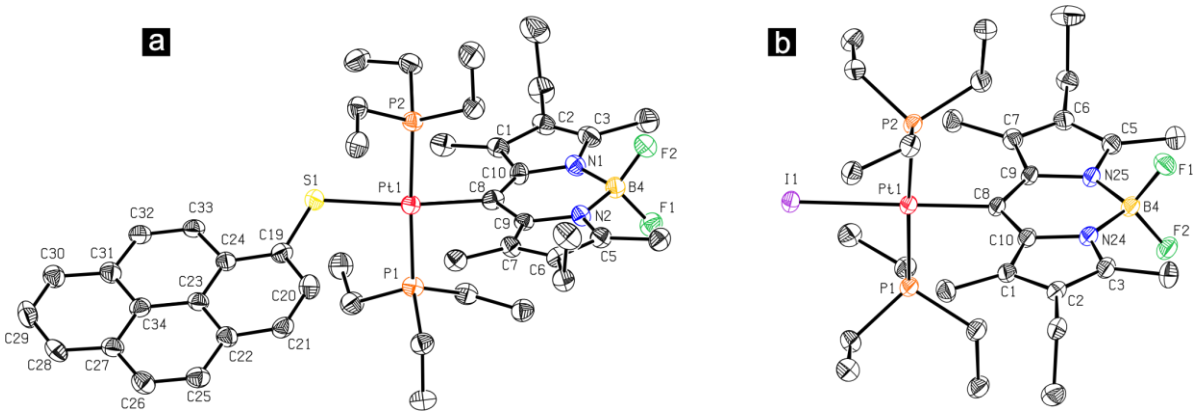

Figure 1. ORTEPs of a) **KBPtSPyr** (only one of the two independent molecules of the units cell is shown) and of b) **KBPtI**. Ellipsoids are drawn on a 40 % probability level. Solvent molecules and protons are omitted for reasons of clarity.

In all complexes, the Pt(II) ion adopts the expected square planar coordination geometry with all *cis*-bond angles close to 90° and the trans-P-Pt-P and I-Pt-C angles close to 180°, whereas the C8-Pt1-S1 angle of 172.7(3)° or 167.9(3)° in **KBPtSPyr** shows larger deviations from ideality. Substitution of the simple BDP ligand of **BPtI** by peralkylated KBDP in **KBPtI** lengthens the Pt-C_{bodipy} and the Pt-I bonds by ca. 0.02 Å, the former probably as the result of increased steric interactions between the alkyl substituents of the PEt_3 and the KBDP ligands, and the latter as the

result of the increased σ-trans-influence of the KBDP ligand.[9] Substitution of the iodo by the 1-mercaptopyrene ligand lengthens the Pt1-C8 bond further by 0.03 Å, which is expected on the basis of the π-accepting character of an S donor ligand and the associated, larger σ-trans-influence. The BDP chromophore is aligned orthogonally to the Pt coordination plane with an interplanar angle of 87.0° to 90°. In contrast, the pyrenyl substituent of **KBPtSPyr** forms an interplanar angle of 70.0° or 73.2° with the Pt coordination plane, such that the interplanar angle between the two chromophores is 19.7° or 18.2° for the two independent molecules of the unit cell. The centroids of the pyrene and BDP dye ligands are 9.96 or 9.80 Å apart. Several intermolecular contacts are found in the crystal packing of **KBPtSPyr**. Details are provided in the Supporting Information.

Photophysical properties.

A common feature of all BDP-Pt-SPyr dyads of this study is that their HOMO is centred on the mercapto-substituted pyrene ligand while their LUMO is essentially bodipy-based. DFT-computed contour diagrams of the relevant MOs of complexes **BPtSPyr**, **BPtSPyrSPtB** and **KBPtSPyr** and the spin densities for their oxidized and reduced forms are displayed as Figures S23 to S28 of the Supporting Information; the respective contributions and spin densities of the individual fragments according to Mulliken analysis are collected in Tables S4 to S11. According to these calculations, both frontier MOs (HOMO, LUMO) of the dyads receive only minor contributions (3% - 7%) from the $Pt(PEt_3)_2$ fragment(s), such that its (their) influence is of a primarily inductive nature. Substitution of the BDP by the more electron donating, peralkylated KBDP and of the terminal mercaptopyrene by the pyrene-1,6-dithiolate ligand induce sizable energy shifts of the LUMO or the HOMO, respectively, as revealed by our electrochemical measurements. Representative voltammograms can be found as Figures S29 to S33 of the Supporting Information, while all pertinent data are collected in Table S12 therein. In brief, substitution of the BDP by the KBDP

ligand shifts the half-wave potential for the bodipy-centred reduction negative (cathodically) by 340 mV, while causing an only minor cathodic shift of 50 mV of the pyrene-based oxidation. *Vice versa*, comparing **BPtSPyr** with **BPtSPyrSPtB** reveals a 190 mV cathodic shift of the oxidation potential, resulting from the attachment of a second $^{-}$S-Pt(PEt_3)$_2$BDP-type donor, while leaving the potential of the BDP-based reduction essentially unaltered.

Figure 2 depicts the UV/Vis spectra of all dyad molecules along with those of suitable reference compounds, which contain only the Pt-BDP or the mercatopyrene moiety. Tabulated data and the corresponding TD-DFT-derived band assignments can be found in Table 2.

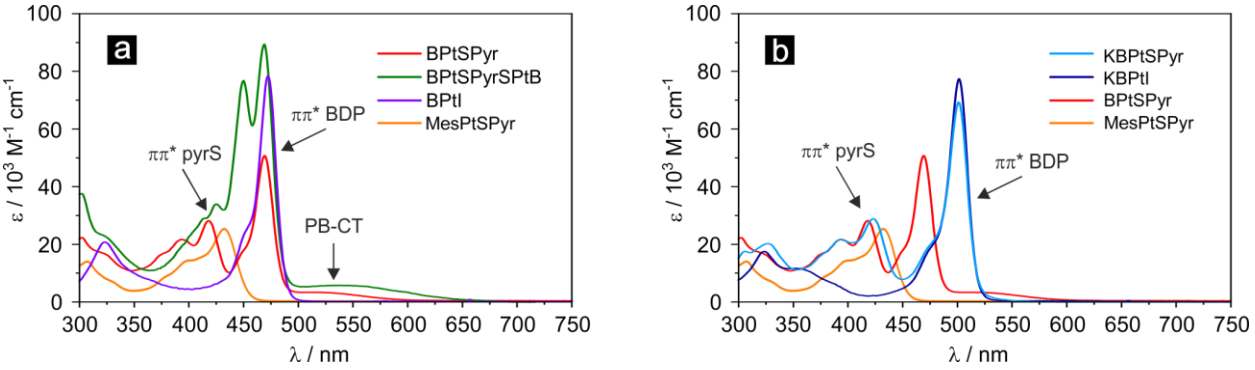

Figure 2. UV/Vis spectra of a) **BPtSPyr**, **BPtSPyrSPtB**, **BPtI** and **MesPtSPyr**, and b) of **KBPtSPyr**, **KBPtI**, **BPtSPyr** and **MesPtSPyr** in toluene.

Complexes **BPtSPyr**, **BPtSPyrSPtB** and **BPtI** with the unsubstituted BDP dye as a σ-bonded ligand exhibit the characteristic BDP-based $^1\pi\pi^*$ absorption band at 470 nm to 490 nm with an extinction coefficient ε of ca. 50×10^3 M^{-1} cm^{-1} for the mononuclear, and of 90×10^3 M^{-1} cm^{-1} for the dinuclear complex with twice the number of BDP chromophores. The electron-donating Pt(PEt_3)$_2$-BDP moieties shift the pyrene-based ππ* absorption bands bathochromically to 375 - 450 nm with a main peak at 418 nm for **BPtSPyr**. They are even more red-shifted in

BPtSPyrSPtB, where they overlap with the BDP absorption. The even lower energy of the main mercaptopyrene ππ* absorption at λ_{max} = 431 nm in the mesityl complex is consistent with this trend and relates to the larger donor capacity of the mesityl ligand. The spectra of **BPtSPyr** and **BPtSPyrSPtB** also feature a broad, solvatochromic (see Figure S34 of the Supporting Information) SPyr-to-BDP charge transfer (PB-CT) band, which is located at ca. 500 nm in toluene solution for **BPtSPyr**.[42] Attachment of a dinegatively charged bridging dithiolate donor and doubling the number of the bodipy acceptors has the effect of shifting the PB-CT band further red to 550 nm and increasing its extinction coefficient (Table 2). The presence of the solvatochromic PB-CT band provides first evidence for optical charge transfer on excitation to generate a charge-separated excited state.

In the complexes **KBPtSPyr** and **KBPtI** with the peralkylated KBDP ligand, the BDP ^{1}ππ* absorption band is red-shifted to 500 nm, and its extinction coefficient is increased to 70×10^3 M^{-1} cm^{-1}. In agreement with the better electron donating properties of the more electron-rich KBDP ligand, the SPyr-based absorption in **KBPtSPyr** is red-shifted by 5 nm (283 cm^{-1}) with respect to **BPtSPyr**, but still blue of that in **MesPtSPyr**. More importantly however, **KBPtSPyr** completely lacks the PB-CT absorption. TD-DFT calculations suggest that such a transition should also be present in **KBPtSPyr**, but is associated with a small oscillator strength and blue shifted by 73 nm (2600 cm^{-1}) compared to **BPtSPyr** (see Figure S25 of the Supporting Information), such that it overlaps with the much more intense KBDP ^{1}ππ* absorption. The blue-shift and the lower oscillator strength of the PB-CT band are immediate consequences of the inferior acceptor properties of the peralkylated BDP ligand. The latter notion is also supported by our electrochemistry data (*vide supra*). Neither of the two major absorption bands of **KBPtSPyr** shows a significant dependence on solvent polarity as is evident from Figure S35 of the Supporting

Information. Importantly, the clear separation of the SPyr and the BDP $^1\pi\pi^*$ transitions in the present dyad systems suggests that the two chromophores are electronically decoupled from each other in the ground state.

Table 2. Absorption data for BPtI, KBPtI, MesPtSPyr, BPtSPyr, BPtSPyrSPtB, and KBPtSPyr as well as TD-DFT-calculated band energies and assignments

absorption data		TD-DFT calculations[a]			
solvent	λ_{max}[b] (ε[c])	λ[b]	f[d]	m.c.[e]	assignment
		BPtI *from ref. 9*			
CH_2Cl_2	322 (12.5), 352 (4.3), 471 (52.6)	295	0.17	H−6 → L (90%)	ππ* BDP
		309	0.07	H−5 → L (81%)	Pt(PEt_3)$_2$ to BDP CT
		392	0.39	H → L (97%)	ππ* BDP
		KBPtI			
toluene	353 (12), 502 (80)	n.d.	n.d.	n.d.	n.d.
THF	351 (9), 500 (74)				
acetone	347 (10), 498 (72)				
		MesPtSPyr *from ref. 42*			
toluene	307 (14), 431 (25)	n.d.	n.d.	n.d.	n.d.
THF	306 (12), 431 (22)				
acetone	430 (23)				
		BPtSPyr *from ref. 42*			
toluene	418 (28), 469 (51), 499 (4)	392	0.37	H-1→L (97%)	ππ* BDP
THF	419 (29), 467 (51), 493 (4)	402	0.66	H→L+1 (95%)	ππ* SPyr
acetone	416 (29), 465 (50), 483 (4)	567	0.05	H→L (99%)	PB-CT
		BPtSPyrSPtB			
toluene	425 (34), 450 (77), 469 (90), 540 (6)	391	0.71	H-3→L+1 (48%), H-2→L (49%)	ππ* BDP
THF	425 (41), 449 (84), 467 (91), 515 (8)	426	0.52	H-1→L+1 (41%), H→L+2 (55%)	ππ* SPyr PB-CT
acetone	424 (38), 448 (76), 465 (88), 475 (8)	433	0.68	H-1→L+1 (53%), H→L+2 (41%)	ππ* SPyr PB-CT
		618	0.08	H→L (97 %)	PB-CT
		KBPtSPyr			
toluene	423 (30), 501 (72)	406	0.68	H→L+1 (95%)	ππ* SPyr
THF	423 (31), 499 (69)	423	0.47	H-1→L (97%)	ππ* BDP
acetone	421 (24), 498 (58)	494	0.03	H→L (98%)	PB-CT

[a]DFT calculations on the pbe1pbe/6-31G(d) level of therory; PCM model for CH_2Cl_2. [b]λ in nm. [c]$\varepsilon \cdot 10^3$ M^{-1} cm^{-1}. [d]f = oscillator strength. [e]m.c. = major contribution. H refers to HOMO and L to LUMO.

Let us now turn to the emission properties of the dyads. In order to aid in the interpretation of their complex, multiple emission features, we will first discuss the corresponding reference compounds with only one type of chromophore. Upon excitation into the SPyr-based $^1\pi\pi^*$ band, **MesPtSPyr** exhibits dual fluorescence and phosphorescence emissions, both at r.t. and at 77 K. Both emissions emanate from the mercaptopyrene ligand as follows from the typical shapes of the emission bands and their associated lifetimes of 1.11 ns and 448 µs to 1 ms (see Figures S36–S42 of the Supporting Information).[42] The observation of phosphorescence indicates that the heavy-metal effect of the attached Pt ion is operative in promoting ISC, similar to Pt complexes with a σ-bonded pyrenyl ligand.[15, 21, 31]

BPtI[9] and **KBPtI** are also dual fluorescence and phosphorescence emitters (see Table 3 and Figure S43 of the Supporting Information). While both exhibit significantly larger phosphorescence quantum yields than **MesPtSPyr**, there are major differences between them. Thus, **KBPtI** is associated with significantly larger fluorescence and lower phosphorescence quantum yields, which attests to less efficient ISC. This is also evident from the increased fluorescence lifetime of 0.96 ns as compared to 0.48 ns for **BPtI** and the derived rate constants k_{ISC} of $2.1\cdot10^9$ for **BPtI** and of $9.4\cdot10^8$ s^{-1} for **KBPtI**. When considering that the two complexes share a common site of platinum attachment to the BDP chromophore and show only small differences in their Pt-C8(bodipy) bond lengths, a reduced external heavy atom effect seems a rather unlikely explanation for the decreased k_{ISC}. We are therefore drawn to the hypothesis that these differences may be due to the more locked, orthogonal conformation of the complexes with the KBDP ligand due to strongly hindered rotation around the Pt-C8(bodipy) bond.

Table 3. Emission data of **BPtSPyr**, **KBPtSPyr** and **BPtSPyrSPtB**

solvent	λ_{exc}[a]	λ_{fl}[b] (assignment)	Φ_{fl}[c]	τ_{fl}[d]	λ_{ph}[b] (assignment)	Φ_{ph}[c]	τ_{ph}[d]
BPtI *from ref.* 9							
CH_2Cl_2	467	481 (^{1}BDP)	0.002	0.48 ± 0.02 ns	641	0.364	297 ± 2 µs
KBPtI							
toluene	485	512	0.10	0.959 ± 0.007 ns	684	0.04	239 ± 2 µs
Me-THF[e]	485	506	n.d.	1.171 ± 0.007 ns	673	n.d.	436 ± 2 µs
MesPtSPyr *from ref.* 42							
toluene	430	460 (^{1} SPyr)	0.24	1.113 ± 0.005 ns	664 (^{3}pyrS)	<0.01	448 ± 6 µs
Me-THF[e]	430	450 (^{1} SPyr)			658 (^{3}pyrS)	n.d.	1.04 ± 0.06 ms
BPtSPyr							
toluene	520				724 (^{3}PB-CT)	0.08	6.7 ± 0.4 µs
	470	484 (^{1}BDP)	n.d.	n.d.	724 (^{3}PB-CT)	0.15	6.7 ± 0.5 µs
	420				724 (^{3}PB-CT)	0.15	6.4 ± 0.3 µs
Me-THF[e]	530 450 415	n.o.			635 (^{3}BDP) 649 (^{3}SPyr)	n.d.	78 ± 0.4 µs 1.12 ± 0.02 ms
KBPtSPyr *from ref.* 42							
toluene	485	512 (^{1}BDP)	<0.01	4.42 ± 0.07 ns	682 (^{3}BDP)	0.03	204 ± 1 µs
	405	n.o.			682 (^{3}BDP)	0.05	203.7 ± 0.9 µs
Me-THF[e]	485	510 (^{1}BDP)	n.d.	2.34 ± 0.05 ns	674 (^{3}BDP)	n.d.	423 ± 2 µs
	405	510 (^{1}BDP)	n.d.	n.d.	674 (^{3}BDP)	n.d.	n.d.
BPtSPyrSPtB							
toluene	550				770 (^{3}PB-CT)	<0.01	32 ± 5 µs
	460	482 (^{1}BDP)	<0.01		635 (^{3}BDP) 760 (^{3}PB-CT)	0.01	178 ± 1 µs 31 ± 2 µs
	420	482 (^{1}BDP)	<0.01	5.0 ± 0.2 ns	653 (^{3}BDP) 760 (^{3}PB-CT)	<0.01	164 ± 12 µs 31 ± 1 µs
Me-THF[e]	550				696 (^{3}SpyrS)	n.d.	369 ± 6 µs
	460	480 (^{1}BDP)	n.d.	n.d.	626 (^{3}BDP) 696 (^{3}SpyrS)	n.d.	499 ± 6 µs 369 ± 3 µs
	420	480 (^{1}BDP)	n.d.	4.1 ± 0.1 ns	626 (^{3}BDP) 696(^{3}SpyrS)	n.d.	479 ± 12 µs 348 ± 2 µs

[a]Excitation wavelength in nm. [b]Wavelength of the fluorescence (fl) or phosphorescence (ph) emissions in nm. [c]Fluorescence (fl) or phosphorescence (ph) quantum yield. [d]Lifetime of the fluorescence (fl) or phosphorescence (ph) emissions. [e]Measured in a 2-MeTHF glass at 77 K.

Importantly, and in contrast to **MesPtSPyr** and **BPtI**, dyad **BPtSPyr** exhibits three different emissions in fluid solution at r.t., depending on the excitation wavelength and solvent polarity. Excitation into the PB-CT absorption band at 520 nm gives rise to a broad and unstructured NIR

emission (see Figure S44a of the Supporting Information) with a quantum yield of 8% in toluene. On increasing the solvent polarity, the emission peak shifts red with a concomitant, drastic decrease of its associated lifetime (see Table S13 of the Supporting Information). When excited into the BDP $^1\pi\pi^*$ absorption band at 470 nm, fluorescence and phosphorescence emissions from the BDP-based $^1\pi\pi^*$ and $^3\pi\pi^*$ excited states add to the emission profile. The latter emissions are hardly influenced by solvent polarity and hence become the dominant features in polar solvents, where the ^{3}PB-CT emission is very weak (Figure 3a). On excitation into the SPyr-based $^1\pi\pi^*$ transition, again solely the ^{3}PB-CT emission can be observed, but with an increased quantum yield of up to 15% at r.t. in toluene solution (Figure S44c of the Supporting Information). This renders **BPtSPyr** an unusually powerful NIR emitter. In a glassy Me-THF matrix at 77 K, only $^3\pi\pi^*$ BDP and pyrene-based $^3\pi\pi^*$[18, 36] emissions are observed, irrespective of the excitation wavelength (Figure 3b).

Dinuclear **BPtSPyrSPyr** has very similar properties to **BPtSPyr**, but shows also subtle differences. As **BPtSPyr**, it emits solely from the ^{3}PB-CT state, when excited into the PB-CT band at 550 nm. In toluene solution, the associated emission wavelength is 770 nm with an associated lifetime of 32 µs (see Figure 3c and S45 of the Supporting Information). Mirroring the trends in the absorption spectra and cyclic voltammetry, the higher electron richness (and hence the higher HOMO energy, *vide supra*) of the bridging pyrene-1,6-dithiolate ligand lowers the energy of the corresponding CT-state with respect to mononuclear **BPtSPyr**. As a consequence, the ^{3}PB-CT emission is red-shifted by 825 cm^{-1} with a concomitant decrease of the quantum yield from 8% to a value of ca. 1%. While one may be drawn to ascribe this decrease in quantum yield to the smaller energy gap to the ground state, in line with the predications of the energy gap law,[45-47] the strongly decreased rate constant for radiationless decay of $k_{nr} = 3.1 \cdot 10^3$ s^{-1} as compared to $k_{nr} = 1 \cdot 10^5$ s^{-1} for

BPtSPyr does not support this view and points to less efficient ISC from the ^{3}PB-CT to the ground state as the underlying reason. No emission from the ^{3}PB-CT state was observed down to 1270 nm in solvents of higher polarity like THF, o-difluorobenzene or acetone.

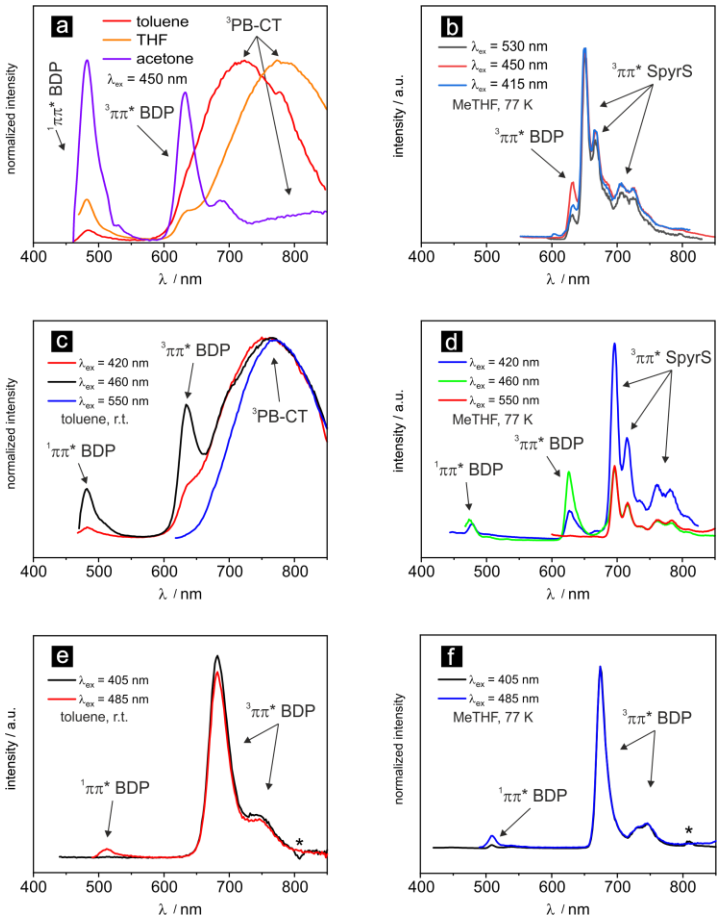

Figure 3. Emission spectra of **BPtSPyr** a) in toluene, THF and acetone at r.t., and b) at 77 K in 2-MeTHF. Emission spectra of **BPtSPyrSPtB** c) at r.t. in toluene, and d) at 77 K in 2-MeTHF. Emission spectra of **KBPtSPyr** e) at r.t. in toluene, and f) at 77 K in 2-MeTHF.

As in **BPtSPyr**, the ^{3}PB-CT emission is complemented by fluorescence and phosphorescence emissions from the BDP-localized ^{1}ππ* and ^{3}ππ* excited states, when irradiated into the BDP ^{1}ππ* band at 460 nm in toluene solution; these are the only emissions in more polar solvents. Associated lifetimes are 5.0 ns and 178 μs, respectively (see Figure S46 for emission spectra and

lifetime decay traces in *o*-$C_6F_2H_4$). At odds with **BPtSPyr**, excitation into the SPyr $^1\pi\pi^*$ band at 420 nm also gives rise to all three emissions. This indicates subtle differences in excited state decay pathways between the two compounds (*vide infra*).

As in fluid solution, emission spectra of **BPtSPyrSPtB** in frozen, glassy matrices at 77 K strongly depend on the excitation wavelength (Figure 3d). Selective irradiation into the ^{3}PB-CT band (λ_{exc} = 550 nm) gives rise to a richly structured emission with a main peak at 696 nm and several vibrational subbands with an associated lifetime of 396 μs. This feature is again identified as phosphorescence from the pyrene-based $^3\pi\pi^*$ state.[15, 21, 31] Mirroring its influence on the energy of the pyrene-localized excited singlet state, the stronger donor substitution of the bridging pyrene-1,6-dithiolate ligand reduces the energy of the $^3\pi\pi^*$ state of the pyrene constituent by 1040 cm^{-1} compared to **BPtSPyr**. As in the fluid solution spectra, excitation into the BDP-based or, to a lesser degree, into the pyrene-based $^1\pi\pi^*$ absorption bands at 460 or 420 nm adds the $^1\pi\pi^*$ and $^3\pi\pi^*$ BDP emissions to the emission profile of **BPtSPyrSPtB** with associated lifetimes of 4.1 ns and 490 μs, respectively (for emission decay traces see Figure S47 of the Supporting Information). All these observations match with the 77 K excitation spectra. Thus, when detecting at the BDP phosphorescence emission at 626 nm, the PB-CT band is absent and the intensity of the $^1\pi\pi^*$ pyrene band is strongly reduced, while all three excitations contribute to the emission from the $^3\pi\pi^*$ state of the pyrene (see Figure S48 of the Supporting Information).

At odds with **BPtSPyr** and **BPtSPyrSPtB**, **KBPtSPyr** shows only the same two emissions as the iodo complexes **BPtI** and **KBPtI**, independent of the excitation wavelength and temperature (compare Figure 3e,f with Figure S43 of the Supporting Information and see Table 3; for emission decay traces see Figures S49-S51 of the Supporting Information). In particular, neither the ^{3}PB-

CT nor the $^3\pi\pi^*$ pyrene emissions are observed. This striking dichotomy is due to the different energies of the corresponding excited states that are involved in the deactivation cascade and energy differences between them. The inductive effect of the alkyl substituents on the KBDP ligand decreases its electron-accepting capability and the energies of the BDP-localized excited singlet and triplet states, which is reflected by their respective red shifts of 1260 cm^{-1} or 980 cm^{-1}. On the other hand, the energy of the $^3\pi\pi^*$ state of the mercaptopyrene ligand is much less affected by substitution of the BDP ligand, such that it remains at an only marginally lower energy than in **BPtSPyr** (Table 3). In this case, the mercaptopyrene ligand acts as an efficient antenna for populating the BPD-localized $\pi\pi^*$ state. Concomitantly, the phosphorescence quantum yield increases to 5% as compared to 3% on direct excitation into the BDP $\pi\pi^*$ band. The absence of any fluorescence emission from the mercaptopyrene and the BDP ligands on excitation at 420 nm likewise attest to efficient ISC from the higher-lying $^1\pi\pi^*$ SPyr to the $^3\pi\pi^*$ KBDP state and the absence of detectable energy transfer from the $^1\pi\pi^*$ SPyr to the $^1\pi\pi^*$ KBDP excited state. Other examples of a direct singlet-to-triplet electron transfer by spin-orbit coupling were already reported in the literature.[48-50] The above conclusions are fully supported by the excitation spectra (see Figure S52 of the Supporting Information). The same overall behaviour also prevails at 77 K.

Our results thus clearly show that the energy levels of the excited singlet and triplet states of either the BDP or the mercaptopyrene ligands as well as those of the PB-CT excited states of both manifolds can be selectively manipulated. This has drastic consequences for the energy cascade underlying the interconversion between the different excited states and their deactivation into the ground state.

An intriguing feature of Pt-BDP complexes is their ability to generate singlet oxygen, sometimes with exceptionally high quantum yields.[9, 33, 34] The amount of singlet oxygen formed in aerated

solutions of the complexes was quantified by comparing the intensity of the $^1O_2$ emission at 1275 nm to that in the presence of tetraphenylporphyrin (TPP) in air-saturated C_6H_6 at r.t. Figure 4 compares the results of this study while Table S14 of the Supporting Information lists the quantum yields Φ_Δ. Quite intriguingly, all complexes of this study produce singlet oxygen. This is particularly true for the simple iodo complex **BPtI**, which, upon excitation into the principal bodipy absorption band, achieves a quantum yield of 94%. In **KBPtI,** the value of Φ_Δ is reduced to 0.65, most probably due to a lower ISC rate constant (*vide supra*). Mononuclear dyads **BPtSPyr** and **KBPtSPyr** also perform well when excited in either the PB-CT or the BDP $\pi\pi^*$ absorption bands, and their quantum yields of 74% are also superior to that of TPP. In contrast to our observation of enhanced quantum yields for ^{3}PB-CT emission, excitation into the $\pi\pi^*$ band of the mercaptopyrene chromophore reduces Φ_Δ to 33 - 40%. **MesPtSPyr**, which lacks a bodipy chromophore, has an even lower quantum yield of 28%. **BPtSPyrSPtB** has the smallest value of Φ_Δ (7-18%, depending on the excitation wavelength). Reasons are the lower ISC rate and a rapid degradation under continuous irradiation of this complex in aerated solutions.

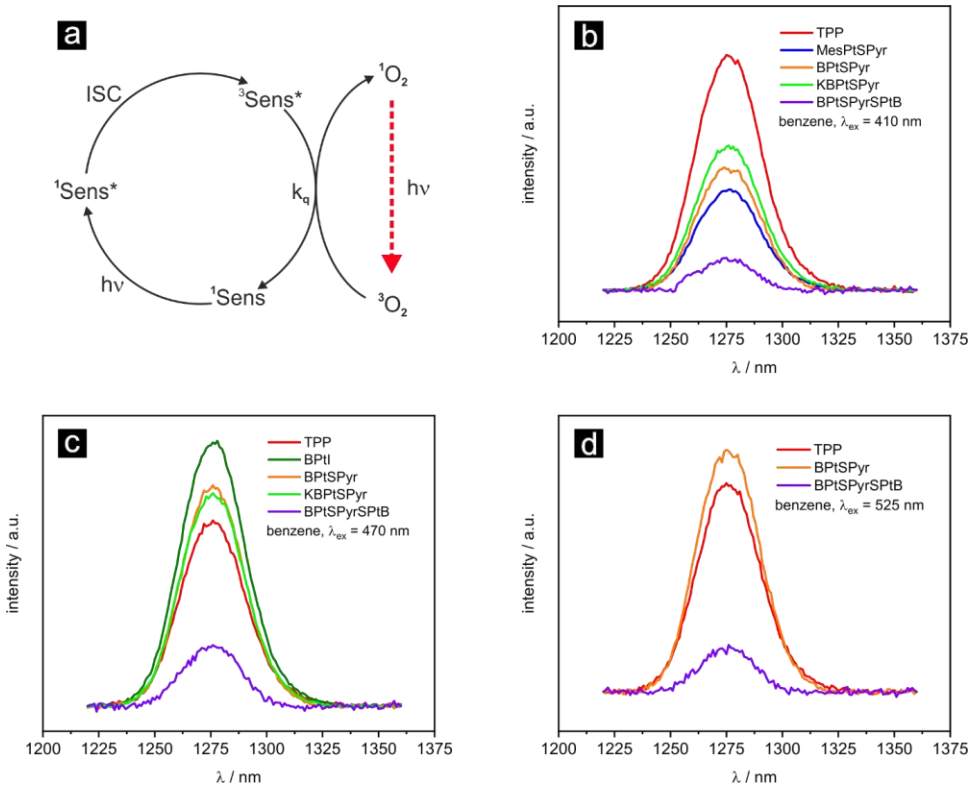

Figure 4. a) Scheme for the generation of singlet oxygen with a triplet sensitizer. b)-d) Singlet oxygen emission upon excitation of the given sensitizers at the stated excitation wavelength at an absorbance of the sensitizer of 0.05 at λ_{exc}.

The chemical reversibility of the oxidations and reductions allowed us to determine the spectroscopic characteristics of the oxidized mercaptopyrene and reduced bodipy ligands, which are both present in the charge-separated states, and to further substantiate our above conclusions. For doing so we resorted to in situ UV/Vis/NIR spectroelectrochemistry inside an optically transparent thin-layer electrolysis cell.[52] Figure 5 displays the results of such measurements for the complexes **BPtSPyr**, **BPtSPyrSPtB** and **KBPtSPyr**, while the corresponding data are summarized in Table S15 of the Supporting Information. Multiple isosbestic points attest to clean interconversions between the different redox forms.

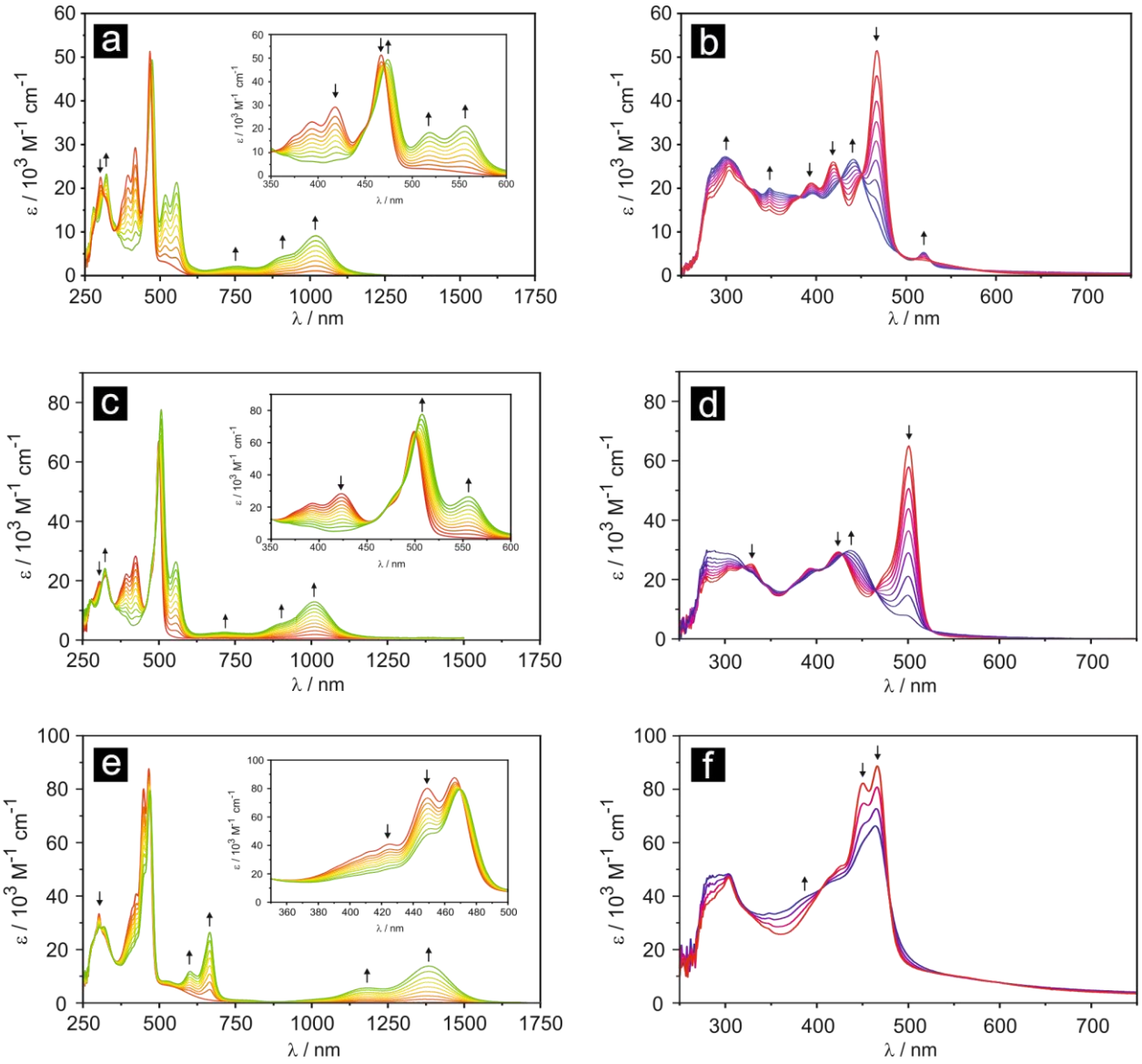

Figure 5. Changes of UV/Vis/NIR spectra of **BPtSPyr** a) on oxidation and b) on reduction; of **KBPtSPyr** c) on oxidation and d) on reduction; as well as that of **BPtSPyrSPtB** e) on oxidation and f) on reduction in THF/0.1 M NBu_4PF_6 or, in the case of 5e) CH_2Cl_2/0.1 M NBu_4PF_6 as the supporting electrolyte at T = 293 K.

Oxidation of these complexes is accompanied by the bleach of the SPyr-based ππ* absorption features while the BDP ππ* band experiences an only minor red-shift. Based on literature data[53, 54] and the results of our TD-DFT calculations on **BPtSPyr**$^{\bullet+}$ (Figure S53 of the Supporting

Information), the new absorption bands at ca. 520, 550, 750, and 1000 nm of **BPtSPyr**$^{\bullet+}$ are safely assigned to ππ* transitions of the oxidized mercatopyrene ligand. The results for **KBPtSPyr**$^{\bullet+}$ are very similar with only minor shifts between these two complexes. The new bands appearing during oxidation of **BPtSPyrSPtB** have the same general appearance but are shifted further red due to the presence of two auxochromic thiolate donors. Reduction of **BPtSPyr** and **KBPtSPyr** in turn bleaches the BDP ππ* band and shifts the SPyr ππ* transition slightly red (Figure 5b and 5d; for a TD-DFT assignment of the bands see Figure S54 of the Supporting Information). Spectral changes upon reduction of **BPtSPyrSPtB** are similar but less characteristic as the BDP and the SPyrS ππ* bands overlap (Figure 5f).

Knowledge of the characteristic absorption features of the Pt-bonded SPyr$^{\bullet+}$ and BDP$^{\bullet-}$ chromophores allows us to identify them in the transient absorption (TA) spectra of the dyads. Figure 6 compares the TA spectra of **BPtI**, **MesPtSPyr**, **BPtSPyr** and **KBPtSPyr** in THF. Associated kinetic traces can be found in Figures S55-S59 of the Supporting Information. **BPtI** shows two TA features when excited at 470 nm (Figure 6a): the bleached BDP signal at 470 nm and, at ca. 400 nm, an excited state absorption (ESA) signal, which we assign to the triplet state of the BDP chromophore.[55-57] The bleach and the ESA features share the same kinetics with two time constants. The longer one of about 149 μs microseconds fits with the corresponding emission data (Table 3 and Figure S55). The shorter lifetime of about 30 μs is most likely due to triplet-triplet annihilation of two molecules of **BPtI** because of the high optical densities required in the TA measurements. On exciting **MesPtSPyr** into its SPyr band at 430 nm, the ground state bleach of the SPyr band and a distinct ESA signal with peaks at 520, 600 and 760 nm are observed. The latter are assigned to the ^{3}ππ* states of the SPyr chromophore and closely resemble those reported

by Pomestchenko *et al.*[36] and Wu *et al.*[58] Again, the kinetics of ground-bleach recovery and ESA decay match with the phosphorescence lifetime (Figure S56 of the Supporting Information).

TA spectra of **BPtSPyr** show three common features, irrespective of the excitation wavelength. These features are the bleaches of the SPyr and BDP ground state absorption signals at ca. 400 nm or 470 nm, and an ESA signal at 550 nm, which we assign to the $SPyr^{\bullet+}$ radical cation (see Figure 5a for comparison). All these features show identical monoexponential decay kinetics with a common time constant of 50 ns when excited at 532 nm (for single wavelength kinetics for each TA feature see Fig. S57 and S58 of the Supporting Information). Excitation into the BDP absorption band at 470 nm leaves the time constants for the features at 415 nm and 550 nm of the SPyr chromophore unchanged, but alters the time constant for recovery of the ground state bleach of the bodipy $^1\pi\pi^*$ band at 475 nm to 16.5 µs, in accordance with the long-lived BDP $^3\pi\pi^*$ excited state in that solvent (red trace in Fig. S57a of the Supporting Information). **BPtSPyrSPtB** was unfortunately not sufficiently photostable to allow for the recording of TA spectra.

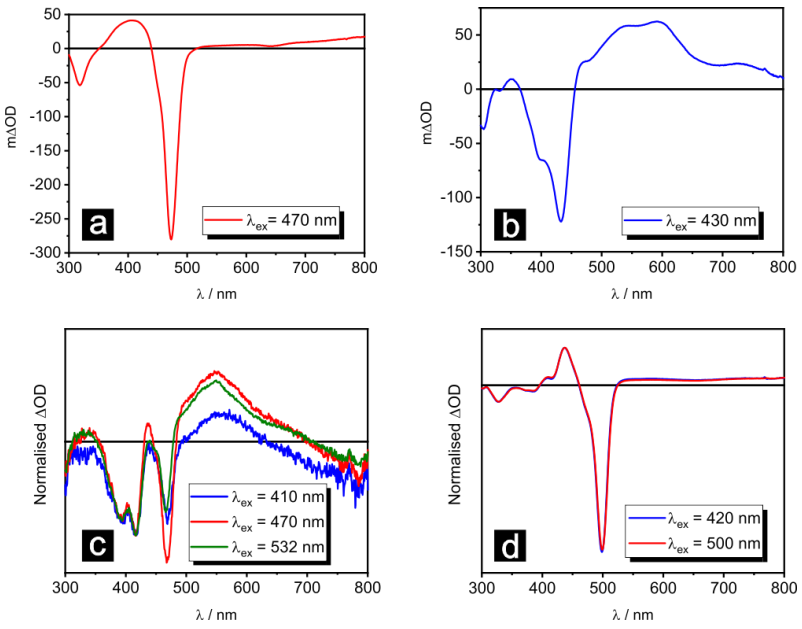

Figure 6. Transient absorption spectra of a) **BPtI**, b) **MesPtSPyr**, c) **BPtSPyr** and d) **KBPtSPyr** in ca. 20 µM THF solutions at r.t. directly after laser excitation at the given wavelength. All spectra are time-integrated over 200 ns.

The TA spectrum of **KBPtSPyr**, which solely emits from excited BDP ππ* states, differs strongly from that of **BPtSPyr** (compare Figures 6c and 6d), but shows close resemblance to that of the parent complex **BPtI**. Following excitations at either 420 nm or 500 nm, an ESA signal at 425 nm is observed in addition to the ground state bleach at 500 nm. The TA spectra of **KBPtSPyr** are thus completely devoid of the ESA signatures of an excited PB-CT or ^{3}ππ* state of the mercaptopyrene ligand. Again, single wavelength kinetics for all TA features agree with the time constant of the phosphorescence emission (see Figure S59 of the Supporting Information).

The differences in the TA spectra of complexes **BPtSPyr** and **KBPtSPyr** thus match with those of their absorption and emission properties. The underlying reason for this dichotomy are the different energies of the various excited states and the concomitant changes of their energy transfer cascades. This is best illustrated with the aid of a schematic Jablonski diagram for **BPtSPyr** in Figure 7. Given the close energetic proximity of three excited states within the singlet and triplet manifolds each and the different degrees of structural reorganization from the initial Frack-Condon states, there is no guarantee that the energy ordering of the structurally relaxed excited states follows that of the corresponding transitions in their absorption or emission spectra. Indeed, test calculations place the BDP-centered ^{1}ππ* state energetically below the ^{1}PB-CT state, although the absorption spectra suggest a different energy ordering. A thorough analysis of this issue, including the identification of the crossing points between the different potential wells, is, however, beyond our present capabilities.

We start our discussion with the emissive properties of **BPtSPyr** at 77 K. Excitation into any absorption band triggers dual phosphorescence emission from the ^{3}ππ* states of the SPyr and the BDP ligands. This signals that the ^{3}PB-CT state is not directly populated from any of the excited singlet states and that all excited states of the singlet manifold relax into these two emissive triplet

states. One possible explanation for this odd behaviour is that the ^{1}PB-CT and ^{3}PB-CT states possess very similar nuclear coordinates and the BDP and SPyr $^3\pi\pi^*$ potential wells have more easily accessible intersections with the ^{1}PB-CT potential well. Similar accounts of a direct singlet-to-triplet electron-transfer by spin–orbit coupling have been published on previous occasions.[48-50]

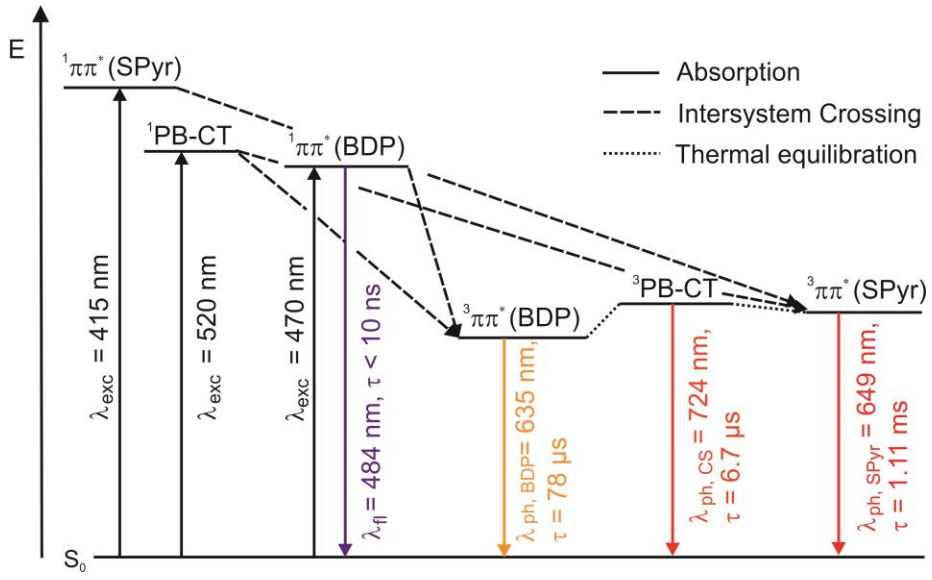

Figure 7. Schematic Jablonski diagrams for **BPtSPyr**. The insert provides electron density difference maps of the individual electronic transitions with decreasing electron density in blue and increasing electron density in red color.

The observed room-temperature emission from the ^{3}PB-CT state is therefore likely due to thermal equilibration of that state with the longer lived BDP- and SPyr-based $^3\pi\pi^*$ states (c. f. the short lifetime of the CT- phosphorescence emission of less than 7 µs). The presence of a competitive deactivation channel for the BDP $^3\pi\pi^*$ state of **BPtSPyr** is also indicated by the significant decrease of its associated lifetime to 78 µs as compared to 279 µs in **BPtI** and 204 µs in **KBPtSPyr**. The latter scenario also explains the further boosting of the quantum yield of the ^{3}PB-CT emission on excitation into the $^1\pi\pi^*$ band of the SPyr ligand and the complete quenching of the associated

pyrene-based phosphorescence at r. t. All these observations strongly suggest that the ^{3}PB-CT state does not constitute the energetically lowest state of the triplet manifold.

The overall behaviour of **BPtSPyrSPtB** is very similar with the exception that the ratio of the time constants for internal conversion from the pyrene-based $^1\pi\pi^*$ state to the $^1\pi\pi^*$ BDP state to that of the ISC to the $^3\pi\pi^*$ state of the pyrenedithiolate ligand is somewhat increased. This allows the BDP-based fluorescence and phosphorescence bands to be observed on irradiation at 420 nm.

Compared to the rather complex characteristics of **BPtSPyr**, that of its peralkylated counterpart **KBPtSPyr** is much simpler. Here, the $^3\pi\pi^*$ BDP state is so much lowered in energy that it is populated from all excited triplet states and no thermal equilibration with the ^{3}PB-CT state occurs.

Summary

We present three dyads of the type *trans*-Pt(σ-BDP)(PEt_3)$_2$(SPyr), where σ-BDP denotes a *meso*-bonded 4,4-difluoro-4-bora-3a,4a-diaza-*s*-indacene (bodipy) dye and SPyr is a mercaptopyrene ligand. Variations over this basic motif are made by exchanging the unsubstituted BDP ligand of **BPtSPyr** by its peralkylated krypto-BDP derivative in **KBPtSPyr**, or by employing either a terminal 1-mercaptopyrene ligand in the mononuclear complexes or a bridging pyrene-1,6-dithiolate ligand in dinuclear **BPtSPyrSPtB**. Our results show that BDP peralkylation has drastic consequences for the energy ordering of the different excited states involved in the deactivation cascades and hence the emissive properties. Thus, **BPtSPyr** and **BPtSPyrSPtB** emit via four different radiative channels, featuring the charge-separated ^{3}PB-CT state and the singlet and triplet BDP-centred ππ* states at r. t., or the BDP and SPyr-centred $^3\pi\pi^*$ states in a frozen matrix at 77 K. Peralkylation of the BDP ligand in **KBPtSPyr** renders the BDP ligand a less strong acceptor. This makes pyrene-to-BDP charge transfer much less exergonic. As a consequence**,**

KBPtSPyr is a dual fluorescence and phosphorescence emitter from the BDP-based $^1\pi\pi^*$ and $^3\pi\pi^*$ states. In this constellation, the SPyr ligand acts as an antenna for the BDP-based excited states. The multitude of potentially emissive states and their various interconnections render the emission profiles of these complexes sensitive to the excitation wavelength, the polarity of the solvent, and the temperature. The interrelations between the various deactivation channels were further probed by transient absorption spectroscopy. UV/Vis/NIR spectroelectrochemistry and comparison to reference compounds with either only the BDP or the SPyr chromophore aid in the assignment of excited state absorption signals.

All complexes act as panchromatic sensitizers for singlet oxygen generation. The mononuclear complexes **BPtI, KBPtSPyr** and **BPtSPyr** outperform the tetraphenylporphyrin standard in this respect.

Electronic supporting information available: ^{1}H, ^{13}C{^{1}H}, and, if applicable, ^{31}P{^{1}H}, ^{195}Pt{^{1}H} NMR spectra of all compounds; Data pertaining to the structure solution and refinement as well as packing diagrams; UV/Vis spectra in different solvents, MO diagrams, TD-DFT computed transitions and electron density difference maps for individual transitions; cyclic voltamnmograms and electrochemistry data; luminescence spectra in different solvents and at different excitation wavelengths as well as time decay traces, computed energies of the frontier MOs; absorption data, MO calculations of relevant MOs, spin densities and MO compositions of the oxidized and reduced forms of the complexes; decay traces for transient spectra of the individual complexes; atomic coordinates of geometry-optimized structures.

Experimental section

Methods. Oxidative addition reactions and ligand manipulations were performed under a N_2 atmosphere using standard Schlenk techniques or inside a glove box. C_6D_6, CD_2Cl_2, $CDCl_3$ and

THF-*d8* were supplied from Eurisotop and stored under N_2-atomosphere over molecular sieves. All other solvents were used as received. Complex *trans*-Pt(bodipy)I(PEt_3)$_2$ (**BPtI**), *trans*-Pt(bodipy)(PEt_3)$_2$(*S*-1-thiopyrene) (**BPtSPyr**) and *trans*-Pt(mesityl)(PEt_3)$_2$(*S*-1-thiopyrene) (**MesPtSPyr**) were synthesized according to the literature protocols.[9, 42]

NMR experiments were carried out on a Varian Unity Inova 400, a Bruker Avance III DRX 400 or a Bruker Avance DRX 600 spectrometer. ^{1}H and ^{13}C spectra were referenced to the solvent signal, while ^{31}P and ^{195}Pt spectra were referenced to external standards (85% H_3PO_4 or saturated $K_2[PtCl_6]$ in D_2O, respectively). NMR data are given as follows: chemical shift (δ in ppm), multiplicity (br, broad; d, doublet; dd, doublet of doublets; m, multiplet; s, singlet; t, triplet, vt virtual triplet), integration, coupling constant (Hz). Unequivocal signal assignments were achieved by 2D NMR experiments. The numbering of the nuclei follows that of the chemical structures displayed at the synthesis protocols.

Combustion analysis was conducted with an Elementar vario MICRO cube CHN-analyzer from Heraeus.

Luminescence spectra and lifetimes as well as quantum yields were measured in acetone, CH_2Cl_2, 2-MeTHF, THF, or toluene solutions of the complex on a PicoQuant FluoTime 300 spectrometer. Unless stated otherwise, absolute quantum yields were determined with an integrating sphere within the FluoTime 300 spectrometer. Emission spectroscopy under inert gas atmosphere was conducted in a quartz cuvette modified with an angle valve from Normag. The emission data of **BPtSPyr** in acetone with excitation at 405 nm are not reported due to sample decomposition upon laser excitation. The singlet oxygen generation quantum yields Φ_Δ were determined by detecting the luminescence signal of singlet oxygen at 1275 nm in air-saturated benzene solution containing the corresponding sensitizer at a concentration to render its

absorbance as 0.05 at λ_{ex}. The integrated intensity of the phosphorescence signal of $^1O_2$ was compared that obtained for a solution containing the reference sensitizer tetraphenylporphyrin (Φ_Δ(TPP) = 0.66),[51] with an absorbance of 0.05 at λ_{ex}.

UV/Vis/NIR spectra were recorded on a TIDAS fiber optic diode array spectrometer (combined MCS UV/NIR and PGS NIR instrumentation) from J&M in HELLMA quartz cuvettes with 0.1 cm optical path lengths.

Transient absorption spectroscopy was performed using an LP920-KS instrument from Edinburgh Instruments. 410 nm and 470 nm excitation were obtained from pulsed third-harmonic radiation from a Quantel Brilliant b Nd:YAG laser equipped with a Rainbow optical parameter oscillator (OPO). 532 nm excitation was obtained from pulsed second-harmonic generation from a Quantel Brilliant b Nd:YAG laser. The laser pulse duration was ~10 ns and the pulse frequency 10 Hz with a typical pulse energy of 7 mJ. Detection of transient absorption spectra occurred on an iCCD camera from Andor. Single-wavelength kinetics were recorded using a photomultiplier tube. All optical spectroscopic experiments were performed under deaerated conditions using quartz cuvettes in which oxygen can be removed by the freeze-pump-thaw technique. Solutions were typically 20 μM in the compound and deaerated through three cycles of freeze-pump-thaw.

All electrochemical experiments were executed in a home-built cylindrical vacuum-tight one-compartment cell. A spiral shaped Pt wire and an Ag wire as the counter and pseudoreference electrodes are sealed into glass capillaries and fixed by Quickfit screws via standard joints. A platinum electrode is introduced as the working electrode through the top port via a Teflon screw cap with a suitable fitting. It is polished with first 1 μm and then 0.25 μm diamond paste before measurements. The cell may be attached to a conventional Schlenk line via a side arm equipped with a Teflon screw valve, allowing experiments to be performed under an argon atmosphere with

approximately 5-7 mL of analyte solution. NBu_4PF_6 (0.1 mM) was used as the supporting electrolyte. Referencing was done with addition of an appropriate amount of decamethylferrocene (Cp^*_2Fe) as an internal standard to the analyte solution after all data of interest had been acquired. Representative sets of scans were repeated with the added standard. Electrochemical data were acquired with a computer-controlled BASi CV50 potentiostat. The optically transparent thin-layer electrochemical (OTTLE) cell was home-built and followed the design of Hartl et al.[52] It comprised a Pt working and counter electrode and a thin silver wire as a pseudoreference electrode sandwiched between two CaF_2 windows of a conventional liquid IR cell with the working electrode positioned in the centre of the spectrometer beam.

Computational Details. The ground-state electronic structures were calculated by density functional theory (DFT) methods using the Gaussian 09[59] program package. Quantum-chemical studies were performed without any symmetry constraints. Open-shell systems were calculated by the unrestricted Kohn−Sham approach.[60] Geometry optimizations followed by vibrational analysis were performed either in a vacuum or in solvent media. The quasi-relativistic Wood−Boring small-core pseudopotentials (MWB),[61, 62] the corresponding optimized set of basis functions[63] for platinum and the halogen atoms, and the 6-31G(d)-polarized double-ζ basis set[64] for the remaining atoms were employed together with the Perdew−Burke−Ernzerhof exchange and correlation functional (PBE0).[65, 66] Solvent effects were accounted for by the polarizable conductor continuum model (PCM)[67-70] with standard parameters for dichloromethane. Absorption spectra and orbital energies were calculated using time-dependent DFT (TD-DFT)[71] with the same functional/basis set combinations as those mentioned above. For an easier comparison with the experiment, the obtained absorption and emission energies were converted into wavelengths and broadened by a

Gaussian distribution (full width at half-maximum = 3000 cm^{-1}) using the program GaussSum.[72] Atomic coordinates of the calculated structures are provided in Tables S16 to S21.

X-ray diffraction analysis of single crystals was performed at 100 K on a STOE IPDS-II diffractometer equipped with a graphite-monochromated radiation source ($\lambda = 0.71073$ Å) and an image plate detection system. A crystal mounted on a fine glass fiber with silicon grease was employed. If not indicated otherwise, the selection, integration, and averaging procedure of the measured reflection intensities, the determination of the unit cell dimensions and a least-squares fit of the 2θ values as well as data reduction, LP-correction and space group determination were performed using the X-Area software package delivered with the diffractometer. A semiempirical absorption correction was performed.[73] All structures were solved by the heavy-atom methods (SHELXS-97,[74] SHELXS-2013,[75] SHELXS-2014[76], or OLEX2[77]). Structure solutions were completed with difference Fourier syntheses and full-matrix last-squares refinements using SHELXL-97,[74] SHELXS-2013,[75] SHELXS-2014,[76] or OLEX2[77] minimizing $\omega(F_o^2 - F_c^2)^2$. The weighted *R* factor (wR^2) and the goodness of the fit GOF are based on F^2. All non-hydrogen atoms were refined with anisotropic displacement parameters, while hydrogen atoms were treated in a riding model. Molecular structures in this work are plotted with PLATON[78] or Mercury.[79] CIF files of the complexes have been deposited at the Cambridge Structure Data Base as CCDC 1908870 (**KBPtI**), and CCDC 1898598 (**KBPtSPyr**) and can be obtained free of charge via www.ccdc.cam.ac.uk/conts/retrieving.html or from the Cambridge Crystallographic Data Center, 12 Union Road, Cambridge CB2 1EZ, U.K.; fax (+44)1223-336-033, or at deposit@ccdc.cam.ac.uk.

Bis-(4-ethyl-3,5-dimethyl-pyrrol-2-yl)-ketone[80]

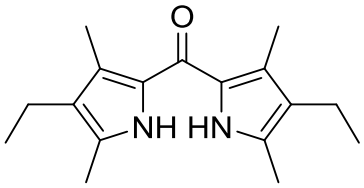

2 ml (14.8 mmol) of 2,4-dimethyl-3-ethyl-pyrrole were dissolved in 40 ml abs. Et_2O and 5.1 ml (15.4 mmol) of a 3 M EtMgBr solution in Et_2O were slowly added at r.t. before heating to reflux for 3 h. After cooling to r.t., 3.9 ml (7.4 mmol) of a 20 % phosgene solution in toluene were added dropwise within 1h. A pale precipitate was observed during addition. The solution was stirred for 72 h at r.t., cooled to 0°C and 60 ml of water were added. Phases were separated and the aqueous phase was extracted with CH_2Cl_2. Combined organic phases were dried over $MgSO_4$ and all volatiles were removed. Recrystallization from 2-propanol and washing with Et_2O gave the product as colorless solid. Yield: 1.00 g, 50 %. ^{1}H NMR (399.79 MHz, $CDCl_3$, 300 K): δ 8.68 (s, 2H, N*H*), 2.42 (q, 4H, $^3J_{HH}$ = 7.5 Hz, C*H*$_2$CH$_3$), 2.25 (s, 6H, C*H*$_3$), 2.17 (s, 6H, C*H*$_3$), 1.09 (t, 6H, $^3J_{HH}$ = 7.5 Hz, CH$_2$C*H*$_3$). ^{13}C NMR (100.54 MHz, $CDCl_3$, 300 K): δ 175.4, 129.8, 127.4, 125.4, 124.4, 17.5, 15.3, 11.5, 10.8.

8-Cloro-2,6-diethyl-1,3,5,7-tetramethyl-bodipy (KBDP)

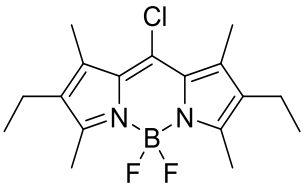

1.0 g (3.7 mmol) of **1** were dissolved in 50 ml of abs. $C_2H_4Cl_2$ and 0.67 ml (7.3 mmol) of $POCl_3$ were added. The mixture was heated to reflux for 2 h, then cooled to 0°C, 5 ml (36.7 mmol) of NEt_3 were added and the solution was stirred for 5 min before adding 5 ml (40.4 mmol) of $BF_3 \cdot Et_2O$ dropwise. The solution was slowly warmed to r.t. and stirred overnight. All volatiles were removed and water was added. The dark mixture was extracted with 4 x 100 ml of Et_2O, the

organic phases were dried over $MgSO_4$ and the solvent was removed. Column chromatography (silica, petrol ether / CH_2Cl_2 2:1, $R_f = 0.25$) yielded the product as a red solid. Yield: 0.53 g, 43 %. ^{1}H NMR (399.79 MHz, $CDCl_3$, 300 K): δ 2.50 (s, 6H, C*H*$_3$), 2.40 (q, 4H, $^3J_{HH}$ = 7.5 Hz, C*H*$_2$CH$_3$), 2.39 (s, 6H, C*H*$_3$), 1.05 (t, 6H, $^3J_{HH}$ = 7.5 Hz, CH$_2$C*H*$_3$). ^{13}C NMR (100.54 MHz, $CDCl_3$, 300 K): δ 153.8, 138.2, 135.3, 133.3, 129.3, 17.2, 14.9, 13.9, 12.6. Anal. Calcd for $C_{17}H_{22}BClF_2N_2$: C, 60.30; H, 6.55; N, 8.27. Found: C, 60.31; H, 6.44; N, 9.42.

cis-Pt(krypto-bodipy)Cl(PEt$_3$)$_2$ (_cis_-KBPtCl)

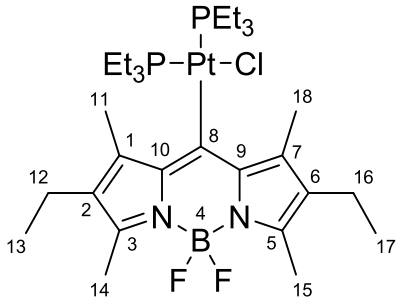

In a flame-dried Schlenk flask 255 µmol Pt(Et)$_2$(PEt$_3$)$_2$ were dissolved in 2 ml of dry degassed benzene. The solution was frozen, evacuated and sealed. Heating of the closed vessel for 2 h to 110°C results in a brown solution. A solution of 278 µmol Cl-bodipy (**2**) in 2 ml of benzene was added at r.t. The solution was kept at 50°C overnight. Filtration of the solid and washing with n-pentane affords the product as a brown solid. Yield: 136 mg, 70%. ^{1}H NMR (399.79 MHz, $CDCl_3$, 300 K): δ 2.90 (s, 6H, H11, H18), 2.41 (s, 6H, H14, H15), 2.36 (q, $^3J_{HH}$ = 7.5 Hz, 4H, H12, H16), 2.06 (m, 6H, P$_{cis}$-C*H*$_2$CH$_3$), 1.71 (m, 6H, P$_{trans}$-C*H*$_2$CH$_3$), 1.17 (m, 9H, P$_{trans}$-CH$_2$C*H*$_3$), 1.01 (t, $^3J_{HH}$ = 7.5 Hz, 6H, H13, H17), 0.93 (m, 9H, P$_{cis}$-CH$_2$C*H*$_3$). ^{13}C {^{1}H} NMR (100.53 MHz, $CDCl_3$, 300 K): δ 147.9 (s, C3, C5), 139.7 (s, C9, C19), 138.1 (s, C1, C7), 130.3 (s, C2, C6), 17.7 (s, C12, C16), 17.4 (dd, J_{PC} = 38.0 Hz, $^4J_{PC}$ = 2.0 Hz, P*C*H$_2$CH$_3$), 16.8 (s, C11, C18), 15.3 (d, J_{PC} = 28.5 Hz, P*C*H$_2$CH$_3$), 15.0 (s, C13, C17), 12.4 (d, J = 4.5 Hz, C14, C15), 7.9 (d, $^2J_{PC}$ =3.9 Hz, PCH$_2$*C*H$_3$),

7.8 (d, $^{2}J_{PC}$ = 2.6 Hz, PCH_2CH_3); the signal for C8 is missing due to low signal to noise ratio. $^{31}P\{^{1}H\}$ NMR (161.84 MHz, $CDCl_3$, 300 K): δ 3.73 (d, $^{2}J_{PP}$ = 17.7 Hz, with satellites J_{PtP} = 1810 Hz), -4.36 (d, $^{2}J_{PP}$ = 17.7 Hz, with satellites J_{PtP} = 3954 Hz). $^{195}Pt\{^{1}H\}$ NMR (85.56 MHz, $CDCl_3$, 300 K): δ -4241 (dd, J_{PtP} = 3954 Hz, 1810 Hz).

***trans*-Pt(krypto-bodipy)I(PEt_3)$_2$ (KBPtI)**

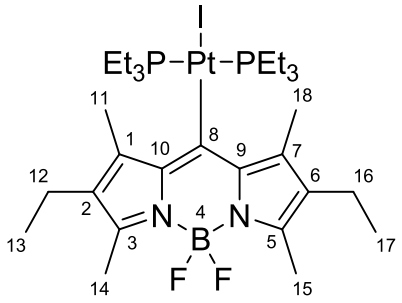

65 µmol of **KBPtCl** and 84 µmol of AgOTf were dissolved in 1 ml of CH_2Cl_2 and heated to reflux for 1h. The filtered solution was added to a methanolic solution of 130 µmol of NaI and stirred for 30 min at r.t. All volatiles were removed and the product was purified by column chromatography (Silica, petrol ether / CH_2Cl_2 1:1, R_f = 0.1). Crystals suitable for X-ray structure analysis were obtained by slow diffusion of pentane into a saturated CH_2Cl_2 solution of the compound at r.t. Yield: 25 mg, 45 %. ^{1}H NMR (399.79 MHz, $CDCl_3$, 300 K): δ 2.93 (s, 6H, H11, H18), 2.41 (s, 6H, H14, H15), 2.39 (q, $^{3}J_{HH}$ = 7.5 Hz, 4H, H12, H16), 1.82 (m, 12H, P-CH_2CH_3), 1.02 (m, 24H, H13, H17, PCH_2CH_3). $^{13}C\{^{1}H\}$ NMR (100.53 MHz, $CDCl_3$, 300 K): δ 161.7 (t, $^{2}J_{PC}$ = 8.5 Hz, C8), 147.9 (s, C3, C5), 138.4 (s with satellites, $^{2}J_{PtC}$ = 32.2 Hz, C9, C10), 137.5 (s with satellites, $^{3}J_{PtC}$ = 23.9 Hz, C1, C7), 131.1 (s, C2, C6), 17.9 (s, C12, C16), 16.0 (vquint, $J_{PC} = {}^{3}J_{PC}$ = 17.2 Hz, with satellites $^{2}J_{PtC}$ = 34.2 Hz, P-CH_2CH_3), 15.3 (s, C11, C18), 14.7 (s, C13, C17), 12.3 (br s, C14, C15), 8.2 (s with satellites, $^{3}J_{PtC}$ = 15.7 Hz, P-CH_2CH_3). $^{31}P\{^{1}H\}$ NMR (161.84 MHz, $CDCl_3$, 300 K): δ -4.90 (s with satellites, J_{PtP} = 2583 Hz). $^{195}Pt\{^{1}H\}$ NMR (85.56 MHz, $CDCl_3$, 300 K): δ -

4432 (t, J_{PtP} = 2583 Hz). Anal. Calcd for $C_{29}H_{52}BF_2IN_2P_2Pt$: C, 40.43; H, 6.08; N, 3.25. Found: C, 40.25; H, 5.90; N, 4.57.

***trans*-Pt(krypto-bodipy)(PEt_3)$_2$(*S*-1-mercaptopyrene) (KBPtSPyr)**

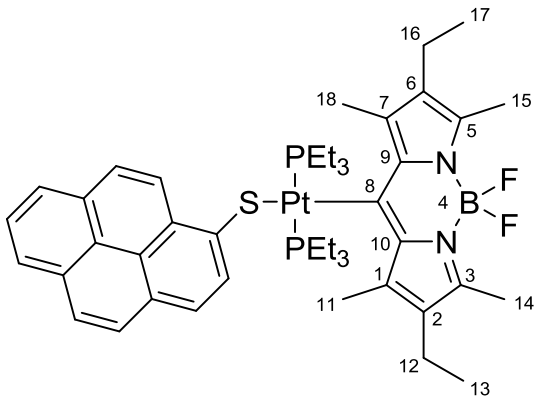

57 µmol of **KBPtCl** and 62 µmol of AgOTf were dissolved in 0.4 ml of dry degassed CD_2Cl_2 in a Young-tube and heated to 40°C for 10 min. ^{31}P NMR spectroscopy indicated full conversion. All volatiles were removed and the remaining solids were dissolved in toluene. 68 µmol pyrene-1-thiol and 91 µmol of diisopropylamine were dissolved in 5 ml dry toluene. The solution containing the Pt complex was filtered and added to the pyrene solution. After stirring for 0.5 h at r.t. the solvent was evaporated. The residue washed with 2 x 10 ml n-pentane and recrystallized twice from a benzene / hexane (1:10) at -25°C. Crystals suitable for X-ray structure analysis were obtained by slow diffusion of pentane into a saturated CH_2Cl_2 solution of the compound at -25°C. Yield: 8.3 mg, 15 %. ^{1}H NMR (399.78 MHz, THF-*d8*, 300 K): δ 9.07 (d, $^3J_{HH}$ = 9.2 Hz, 1H, H_{Pyr}), 8.42 (d, $^3J_{HH}$ = 8.0 Hz, 1H, H_{Pyr}), 8.06 (d, $^3J_{HH}$ = 7.5 Hz, 1H, H_{Pyr}), 8.01 (m, 2H, H_{Pyr}), 7.88 (m, 3H, H_{Pyr}), 7.83 (d, $^3J_{HH}$ = 8.8 Hz, 1H, H_{Pyr}), 3.29 (s, 6H, H11, H18), 2.49 (q, $^3J_{HH}$ = 7.6 Hz, 4H, H12, H16), 2.39 (s, 6H, H14, H15), 1.75 (m, 12H, PC*H*$_2$CH$_3$), 1.10 (t, $^3J_{HH}$ = 7.6 Hz, 4H, H13, H17), 0.92 (m, 18H, PCH$_2$C*H*$_3$). ^{13}C {^{1}H} NMR (100.53 MHz, THF-*d8*, 300 K): δ 169.0 (t, $^2J_{PC}$ =

9.0 Hz, C8), 148.0 (s, C3, C5), 145.8 (s, C_{Pyr}), 141.0 (s, C9, C10), 137.9 (s, C1, C7), 133.3 (s, C_{Pyr}), 133.0 (s, C_{Pyr}), 132.9 (s, C_{Pyr}), 132.3 (s, C_{Pyr}), 131.4 (s, C3, C6), 128.5 (s, C_{Pyr}), 128.0 (s, C_{Pyr}), 127.7 (s, C_{Pyr}), 126.8 (s, C_{Pyr}), 126.64 (s, C_{Pyr}), 126.62 (s, C_{Pyr}), 126.2 (s, C_{Pyr}), 125.5 (s, C_{Pyr}), 124.7 (s, C_{Pyr}), 124.6 (s, C_{Pyr}), 124.4 (s, C_{Pyr}), 18.6 (s, C12, C16), 17.0 (s, C11, C18), 15.8 (t, J_{PC} = 16.9 Hz, P*C*H_2CH_3), 15.2 (s, C13, C17), 12.4 (s, C14, C15), 8.2 (s, PCH_2CH_3). ^{31}P {^1H} NMR (161.83 MHz, C_6D_6, 300 K): δ -2.63 (s with satellites, J_{PtP} = 2611 Hz). ^{195}Pt {^1H} NMR (85.55 MHz, C_6D_6, 300 K): δ -4249 (t, J_{PtP} = 2611 Hz). HR ESI-MS Calcd for [$(C_{45}H_{61}BF_2N_2P_2PtS)^+$]: *m/z* 967.3732. Found: m/z 967.3549.

***trans*-Pt$_2$(bodipy)$_2$(PEt$_3$)$_4$(*S*,*S'*-1,6-dimercaptopyrene) (BPtSPyrSPtB)**

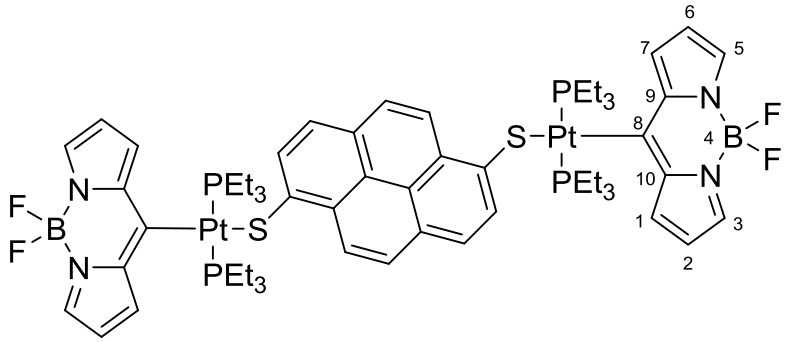

Under an atmosphere of nitrogen 119 mg (169 µmol) of **BPtBr** and 65 mg (254 µmol) of AgOTf were dissolved in 0.6 ml CD_2Cl_2 and heated to reflux for 20 min. After reaction control by ^{31}P NMR spectroscopy the solvent was removed, the residue re-dissolved in 5 ml of benzene and filtered. This solution was added to a mixture containing 23mg (85 µmol) of 1,6-dimercaptopyrene and 24 µl (170 µmol) of $^{i}Pr_2NH$ in 5 ml of toluene. After 90 min all volatiles were removed and the product was washed with 1 x 5 ml benzene, 2 x 5 ml MeOH, 2 x 5 ml Et_2O and 2 x 5 ml *n*-pentane. The product was obtained as a brown solid. Yield: 57 mg, 45 %. ^1H NMR (399.78 MHz, THF-*d8*, 300 K): δ 8.80 (d, $^3J_{HH}$ = 9.2 Hz, 1H, H_{pyr}), 8.68 (d, $^3J_{HH}$ = 7.9 Hz, 1H, H_{pyr}), 7.92 (d,

$^{3}J_{HH}$ = 7.9 Hz, 1H, H_{pyr}), 7.88 (d, $^{3}J_{HH}$ = 9.2 Hz, 1H, H_{pyr}), 7.68 (br s, 4H, H3, H5), 7.65 (d, $^{3}J_{HH}$ = XY Hz, 4H, H1, H7), 6.51 (dd, $^{3}J_{HH}$ = XY Hz, $^{3}J_{HH}$ = XY Hz, 4H, H2, H6), 1.78 (m, 24 H, PCH_2CH_3), 1.01 (m, 36 H, PCH_2CH_3). ^{13}C {^{1}H} NMR (150.97 MHz, THF-*d8*, 298 K): δ 188.3 (s, C8), 144.5 (s, C7/10, S-C_{pyr}), 137.9 (s, C3, C5), 133.6 (s, with shoulders, C1, C7), 133.2 (s, C_{pyr}), 132.1 (s, C_{pyr}), 128.7 (s, C_{pyr}), 127.2 (s, C_{pyr}), 126.8 (s, C_{pyr}), 124.8 (s, C_{pyr}), 123.2 (s, C_{pyr}), 116.5 (s, C2, C6), 14.8 (t, J_{PC} = 17.2 Hz, PCH_2CH_3), 8.3 (s, PCH_2CH_3). ^{31}P {^{1}H} NMR (161.83 MHz, THF-*d8*, 300 K): δ 6.46 (s, with satellites, J_{PtP} = 2493 Hz). ^{195}Pt {^{1}H} NMR (85.56 MHz, $CDCl_3$, 300 K): δ -4344 (t, J_{PtP} = 2491 Hz). Anal. Calcd for $C_{58}H_{80}B_2F_4N_4P_4Pt_2S_2$: C, 46.16; H, 5.34; N, 3.71; Found: C, 44.70; H, 5.32; N, 4.60.

Notes

The authors declare no competing financial interest.

Acknowledgements

We gratefully acknowledge financial support of this work by the Deutsche Forschungsgemeinschaft (DFG, grant number Wi1262/10-2) and the Swiss national Science Foundation (grant number 200021_176780). We also wish to thank the reviewers for their insightful comments.

References

1. M. Bachmann, O. Blacque and K. Venkatesan, *Chem. Eur. J.*, 2017, **23**, 9451-9456.
2. Y. Yang, M. Lowry, C. M. Schowalter, S. O. Fakayode, J. O. Escobedo, X. Xu, H. Zhang, T. J. Jensen, F. R. Fronczek, I. M. Warner and R. M. Strongin, *J. Am. Chem. Soc.*, 2006, **128**, 14081-14092.
3. S. Park, J. E. Kwon, S. H. Kim, J. Seo, K. Chung, S. Y. Park, D. J. Jang, B. Milian Medina, J. Gierschner and S. Y. Park, *J. Am. Chem. Soc.*, 2009, **131**, 14043-14049.
4. Y. Liu, M. Nishiura, Y. Wang and Z. Hou, *J. Am. Chem. Soc.*, 2006, **128**, 5592-5593.
5. Y. Liu, H. Guo and J. Zhao, *Chem. Commun.*, 2011, **47**, 11471-11473.
6. H. Xiang, L. Zhou, Y. Feng, J. Cheng, D. Wu and X. Zhou, *Inorg. Chem.*, 2012, **51**, 5208-5212.

7. H. Hochreiner, I. Sanchez-Barragan, J. M. Costa-Fernandez and A. Sanz-Medel, *Talanta*, 2005, **66**, 611-618.
8. F. Geist, A. Jackel and R. F. Winter, *Inorg. Chem.*, 2015, **54**, 10946-10957.
9. P. Irmler and R. F. Winter, *Dalton Trans.*, 2016, **45**, 10420-10434.
10. M. A. El-Sayed, *J. Chem. Phys.*, 1963, **38**, 2834-2838.
11. E. Yu-Tzu Li, T. Y. Jiang, Y. Chi and P. T. Chou, *Phys. Chem. Chem. Phys.*, 2014, **16**, 26184-26192.
12. P.-T. Chou, Y. Chi, M.-W. Chung and C.-C. Lin, *Coord. Chem. Rev.*, 2011, **255**, 2653-2665.
13. M. Montalti, A. Credi, L. Prodi and M. Teresa Gandolfi, *Handbook of Photochemistry*, CRC Press, Boca Raton, 3rd edn., 2006.
14. S. P. McGlynn, T. Azumi and M. Kinoshita, *Molecular Spectroscopy of the Triplet State*, Prentice-Hall, Englewood Cliffs, N.J, 1969.
15. W. Y. Heng, J. Hu and J. H. K. Yip, *Organometallics*, 2007, **26**, 6760-6768.
16. C. C. Hsu, C. C. Lin, P. T. Chou, C. H. Lai, C. W. Hsu, C. H. Lin and Y. Chi, *J. Am. Chem. Soc.*, 2012, **134**, 7715-7724.
17. C.-W. Hsu, C.-C. Lin, M.-W. Chung, Y. Chi, G.-H. Lee, P.-T. Chou, C.-H. Chang and P.-Y. Chen, *J. Am. Chem. Soc.*, 2011, **133**, 12085-12099.
18. E. O. Danilov, I. E. Pomestchenko, S. Kinayyigit, P. L. Gentili, M. Hissler, R. Ziessel and F. N. Castellano, *J. Phys. Chem. A*, 2005, **109**, 2465-2471.
19. B. Ma, P. I. Djurovich, M. Yousufuddin, R. Bau and M. E. Thompson, *J. Phys. Chem. C*, 2008, **112**, 8022-8031.
20. W. Yang, A. Karatay, J. Zhao, J. Song, L. Zhao, Y. Xing, C. Zhang, C. He, H. G. Yaglioglu, M. Hayvali, A. Elmali and B. Kucukoz, *Inorg. Chem.*, 2015, **54**, 7492-7505.
21. W. Wu, W. Wu, S. Ji, H. Guo and J. Zhao, *Eur. J. Inorg. Chem.*, 2010, **2010**, 4470-4482.
22. A. J. Hallett, N. White, W. Wu, X. Cui, P. N. Horton, S. J. Coles, J. Zhao and S. J. Pope, *Chem. Commun.*, 2012, **48**, 10838-10840.
23. A. F. Morales, G. Accorsi, N. Armaroli, F. Barigelletti, S. J. A. Pope and M. D. Ward, *Inorg. Chem.*, 2002, **41**, 6711-6719.
24. N. D. McClenaghan, Y. Leydet, B. Maubert, M. T. Indelli and S. Campagna, *Coord. Chem. Rev.*, 2005, **249**, 1336-1350.
25. K. Oppelt, D. A. M. Egbe, U. Monkowius, M. List, M. Zabel, N. S. Sariciftci and G. Knör, *J. Organomet. Chem.*, 2011, **696**, 2252-2258.
26. R. Liu, N. Dandu, Y. Li, S. Kilina and W. Sun, *Dalton Trans.*, 2013, **42**, 4398-4409.
27. A. J. Howarth, M. B. Majewski and M. O. Wolf, *Coord. Chem. Rev.*, 2015, **282-283**, 139-149.
28. I. E. Pomestchenko and F. N. Castellano, *J. Phys. Chem. A*, 2004, **108**, 3485-3492.
29. T. Tsuboi, D.-F. Huang, T. J. Chow and W. Huang, *Opt. Mater.*, 2014, **36**, 1734-1738.
30. J. Brooks, Y. Babayan, S. Lamansky, P. I. Djurovich, I. Tsyba, R. Bau and M. E. Thompson, *Inorg. Chem.*, 2002, **41**, 3055-3066.
31. J. Hu, J. H. K. Yip, D.-L. Ma, K.-Y. Wong and W.-H. Chung, *Organometallics*, 2009, **28**, 51-59.
32. F. Geist, A. Jackel and R. F. Winter, *Dalton Trans.*, 2015, **44**, 3974-3987.
33. P. Irmler and R. F. Winter, *Organometallics*, 2018, **37**, 235-253.
34. F. Geist, A. Jackel, P. Irmler, M. Linseis, S. Malzkuhn, M. Kuss-Petermann, O. S. Wenger and R. F. Winter, *Inorg. Chem.*, 2017, **56**, 914-930.

35. N. Kanamaru, H. R. Bhattacharjee and E. C. Lim, *Chem. Phys. Lett.*, 1974, **26**, 174-179.
36. I. E. Pomestchenko, C. R. Luman, M. Hissler, R. Ziessel and F. N. Castellano, *Inorg. Chem.*, 2003, **42**, 1394-1396.
37. J. P. Rostron, G. Ulrich, P. Retailleau, A. Harriman and R. Ziessel, *New J. Chem.*, 2005, **29**, 1241.
38. R. Ziessel, C. Goze, G. Ulrich, M. Cesario, P. Retailleau, A. Harriman and J. P. Rostron, *Chem. Eur. J.*, 2005, **11**, 7366-7378.
39. X. F. Zhang and N. Feng, *Chem. Asian J.*, 2017, **12**, 2447-2456.
40. M. A. Filatov, S. Karuthedath, P. M. Polestshuk, H. Savoie, K. J. Flanagan, C. Sy, E. Sitte, M. Telitchko, F. Laquai, R. W. Boyle and M. O. Senge, *J. Am. Chem. Soc.*, 2017, **139**, 6282-6285.
41. M. A. Filatov, S. Karuthedath, P. M. Polestshuk, S. Callaghan, K. J. Flanagan, M. Telitchko, T. Wiesner, F. Laquai and M. O. Senge, *Phys. Chem. Chem. Phys.*, 2018, **20**, 8016-8031.
42. P. Irmler, F. S. Gogesch, C. B. Larsen, O. S. Wenger and R. F. Winter, *Dalton Trans.*, 2019, **48**, 1171-1174.
43. T. J. McCarthy, R. G. Nuzzo and G. M. Whitesides, *J. Am. Chem. Soc.*, 1981, **103**, 3396-3403.
44. M. A. Cairns, K. R. Dixon and G. A. Rivett, *J. Organomet. Chem.*, 1979, **171**, 373-385.
45. J. S. Wilson, N. Chawdhury, M. R. A. Al-Mandhary, M. Younus, M. S. Khan, P. R. Raithby, A. Köhler and R. H. Friend, *J. Am. Chem. Soc.*, 2001, **123**, 9412-9417.
46. C. E. Whittle, J. A. Weinstein, M. W. George and K. S. Schanze, *Inorg. Chem.*, 2001, **40**, 4053-4062.
47. E. M. Kober, J. V. Caspar, R. S. Lumpkin and T. J. Meyer, *J. Phys. Chem.*, 1986, **90**, 3722-3734.
48. M. R. Wasielewski, D. G. Johnson, W. A. Svec, K. M. Kersey and D. W. Minsek, *J. Am. Chem. Soc.*, 1988, **110**, 7219-7221.
49. S.-H. Lee, A. G. Larsen, K. Ohkubo, Z.-L. Cai, J. R. Reimers, S. Fukuzumi and M. J. Crossley, *Chem. Sci.*, 2012, **3**, 257-269.
50. T. Higashino, T. Yamada, M. Yamamoto, A. Furube, N. V. Tkachenko, T. Miura, Y. Kobori, R. Jono, K. Yamashita and H. Imahori, *Angew. Chem. Int. Ed. Engl.*, 2016, **55**, 629-633.
51. F. Wilkinson, W. P. Helman and A. B. Ross, *J. Phys. Chem. Ref. Data*, 1993, **22**, 113-262.
52. M. Krejčik, M. Daněk and F. Hartl, *J. Electroanal. Chem.* 1991, **317**, 179-187.
53. T. Shida and S. Iwata, *J. Am. Chem. Soc.*, 1973, **95**, 3473-3483.
54. J. Maurer, M. Linseis, B. Sarkar, B. Schwederski, M. Niemeyer, W. Kaim, S. Zalis, C. Anson, M. Zabel and R. F. Winter, *J. Am. Chem. Soc.*, 2008, **130**, 259-268.
55. R. P. Sabatini, T. M. McCormick, T. Lazarides, K. C. Wilson, R. Eisenberg and D. W. McCamant, *J. Phys. Chem. Lett.*, 2011, **2**, 223-227.
56. X. F. Zhang and X. Yang, *J. Phys. Chem. B*, 2013, **117**, 5533-5539.
57. Z. Wang and J. Zhao, *Org. Lett.*, 2017, **19**, 4492-4495.
58. W. Wu, J. Sun, S. Ji, W. Wu, J. Zhao and H. Guo, *Dalton Trans.*, 2011, **40**, 11550-11561.
59. M. J. Frisch, G. W. Trucks, H. B. Schlegel, G. E. Scuseria, M. A. Robb, J. R. Cheeseman, G. Scalmani, V. Barone, B. Mennucci, G. A. Petersson, H. Nakatsuji, M. Caricato, X. Li, H. P. Hratchian, A. F. Izmaylov, J. Bloino, G. Zheng, J. L. Sonnenberg, M. Hada, M.

Ehara, K. Toyota, R. Fukuda, J. Hasegawa, M. Ishida, T. Nakajima, Y. Honda, O. Kitao, H. Nakai, T. Vreven, J. A. Montgomery Jr., J. E. Peralta, F. Ogliaro, M. J. Bearpark, J. Heyd, E. N. Brothers, K. N. Kudin, V. N. Staroverov, R. Kobayashi, J. Normand, K. Raghavachari, A. P. Rendell, J. C. Burant, S. S. Iyengar, J. Tomasi, M. Cossi, N. Rega, N. J. Millam, M. Klene, J. E. Knox, J. B. Cross, V. Bakken, C. Adamo, J. Jaramillo, R. Gomperts, R. E. Stratmann, O. Yazyev, A. J. Austin, R. Cammi, C. Pomelli, J. W. Ochterski, R. L. Martin, K. Morokuma, V. G. Zakrzewski, G. A. Voth, P. Salvador, J. J. Dannenberg, S. Dapprich, A. D. Daniels, Ö. Farkas, J. B. Foresman, J. V. Ortiz, J. Cioslowski and D. J. Fox, *Gaussian 09, Revision C.01*, Gaussian Inc., Wallingford, CT, USA, 2009.

60. O. Gunnarsson and B. I. Lundqvist, *Phys. Rev. B*, 1976, **13**, 4274-4298.
61. W. Küchle, M. Dolg, H. Stoll and H. Preuss, *J. Chem. Phys.*, 1994, **100**, 7535-7542.
62. M. Dolg, H. Stoll and H. Preuss, *J. Chem. Phys.*, 1989, **90**, 1730.
63. D. Andrae, U. Häußermann, M. Dolg, H. Stoll and H. Preuss, *Theor. Chim. Acta*, 1990, **77**, 123-141.
64. P. C. Hariharan and J. A. Pople, *Theor. Chim. Acta*, 1973, **28**, 213-222.
65. J. P. Perdew, K. Burke and M. Ernzerhof, *Phys. Rev. Lett.*, 1996, **77**, 3865-3868.
66. C. Adamo and V. Barone, *J. Chem. Phys.*, 1999, **110**, 6158-6170.
67. E. Cancés, B. Mennucci and J. Tomasi, *J. Chem. Phys.*, 1997, **107**, 3032-3041.
68. B. Mennucci and J. Tomasi, *J. Chem. Phys.*, 1997, **106**, 5151-5158.
69. M. Cossi, N. Rega, G. Scalmani and V. Barone, *J. Comput. Chem.*, 2003, **24**, 669-681.
70. G. Scalmani and M. J. Frisch, *J. Chem. Phys.*, 2010, **132**, 114110.
71. E. Runge and E. K. U. Gross, *Phys. Rev. Lett.*, 1984, **52**, 997-1000.
72. N. M. O'Boyle, A. L. Tenderholt and K. M. Langner, *J. Comput. Chem.*, 2008, **29**, 839-845.
73. W. Herrendorf and W. Bärnighausen, *X-Area, Version 1.06*, Stoe, Darmstadt, 1999.
74. G. M. Sheldrick, *Program for Crystal Structure Solution and Refinement*, University of Göttingen, Germany, 1997.
75. G. M. Sheldrick, *Acta Cryst. A*, 2008, **64**, 112-122.
76. G. M. Sheldrick, *Acta Crystallogr. A*, 2008, **64**, 112-122.
77. O. V. Dolomanov, L. J. Bourhis, R. J. Gildea, J. A. K. Howard and H. Puschmann, *J. Appl. Crystallogr.*, 2009, **42**, 339-341.
78. A. L. Spek, *Acta Cryst. D*, 2009, **65**, 148-155.
79. C. F. Macrae, I. J. Bruno, J. A. Chisholm, P. R. Edgington, P. McCabe, E. Pidcock, L. Rodriguez-Monge, R. Taylor, J. van de Streek and P. A. Wood, *J. Appl. Crystallogr.*, 2008, **41**, 466-470.
80. H. Fischer and H. Orth, *Ann. Chem.*, 1933, **502**, 237-264.

TOC graphic

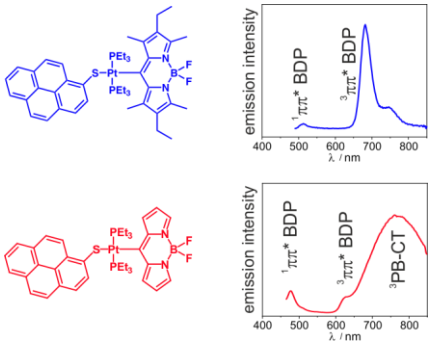

Text for graphical abstract:

Pt(σ-bodipy)(mercaptopyrene) dyads offer several emissions emanating from the bodipy and the mercaptopyrene ππ* states as well as NIR phosphorescence from a pyrene-to-bodipy charge-transfer state. The energy ordering of these states and the emission profile can be manipulated by peralkylation of the bodipy ligand.